Equivalent Lateral Force Design Method for Longitudinal Buckling-Restrained Braces in Bidirectional Ductile Diaphragms

Homero Carrion-Cabrera, M.ASCE[1]; and Michel Bruneau, Dist.M.ASCE[2]

Abstract: Bridge design specifications include design provisions for ductile diaphragms to resist seismic excitations perpendicular to a bridge's axis. Buckling restrained braces (BRBs) can conveniently be used for this purpose. Bidirectional ductile diaphragms expand the concept to resist all-direction seismic forces, and nonlinear inelastic response history analyses (NL-RHAs) can be used to show that satisfactory seismic performance objectives can be obtained using this concept. However, a simple design procedure is needed to address the design of the BRBs in the bridge longitudinal direction. As a first step, to fill that need for common multispan simply-supported bridges, a relatively simple-to-use equivalent lateral force (ELF) procedure has been developed on the basis of results from "optimal designs" obtained using NL-RHAs. Findings indicate that the proposed ELF design procedure leads to design that meet the target design objectives.
DOI: 10.1061/JSENDH.STENG-12846.

Author keywords: Buckling restrained braces (BRBs); Resilient bridges; Seismic design; Inelastic behavior; Ductile response; Full functionality.

Introduction

Seismic design of common multi-span bridges generally relies either on plastic hinging of columns to dissipate earthquake energy, or on base isolation. The first one implies damage to the gravity-carrying columns (Lehman and Moehle 2000); the second one requires a special bearings and expansion joints to accommodate displacements that can be extremely large in many cases (Roussis et al. 2003). Using the bidirectional ductile end diaphragm (BDDD) concept with inexpensive buckling restrained braces (BRBs) can provide resilient bridges with damage-free columns, at low cost, while minimizing displacements demands to levels that can be easily accommodated.

BRBs (Bruneau et al. 2011; Watanabe et al. 1988) have been used in some large bridges (Kanaji et al. 2005; Lanning 2014; Lanning et al. 2016a, b; Reno and Pohll 2010; Wang et al. 2016) and structural engineers are already familiar with BRBs in building applications (Aiken et al. 2002; Cui 2020; Fahnestock et al. 2007; Guerrero et al. 2016; Hoveidae and Rafezy 2012; Kiggins and Uang 2006; López and Sabelli 2004; MacRae et al. 2021; Sabelli et al. 2003; Saxey 2015; Tremblay et al. 2006; Tsai and Hsiao 2008; Tsai et al. 2008; Uang et al. 2004).

Currently, if wishing to use BRBs to implement a ductile diaphragm strategy, the AASHTO Guide Specification for LRFD Seismic Bridge Design (AASHTO 2011) provides simple equations that could be used to resist seismic excitations only in the direction transverse to the bridge axis, based on development and validation work by Zahrai and Bruneau (1999a, b), Alfawakhiri and Bruneau (2001), and Carden et al. (2006). The concept was expanded to address bidirectional seismic forces for bridges with stiff structures (Celik and Bruneau 2009; Wei and Bruneau 2018) and a design procedure was also provided for the case of rigid piers. However, while the concept of *bidirectional ductile end diaphragm* emphasizes the ability to dissipate energy under both longitudinal and transverse seismic excitations by devices installed at the ends of the span, there is no verified design procedure available other than performing NL-RHA (Lanning 2014; Lanning et al. 2016b) to design BRBs in the longitudinal direction. Pantelides et al. (2016) studied the application of BRBs in the longitudinal direction to reduce pounding in curved and skewed bridges as a retrofit strategy but did not propose a generally applicable elastic analysis based design procedure.

To make the bidirectional diaphragm concept attractive to be applied to common multispan bridges, a design procedure based on elastic analysis is required. Carrion-Cabrera and Bruneau (2022b) showed, using nonlinear response history analysis (NL-RHA), that using the response spectrum analysis (RSA) for design for the longitudinal BRBs in BDDD can be effective to limit the maximum ductility demand in BRBs in the bridge, but also that only a few BRBs reached the set target ductility in such designs (they also showed that the NL-RHA approach used provided acceptable results by studying the sensitivity of the bridges response to the use of different BRB material models themselves calibrated against test results of BRBs). Carrion-Cabrera and Bruneau (2022a) then showed that NL-RHA could be used to achieve an optimum design whereby all BRBs reach the same target ductility demand, but this design approach is time consuming and computationally demanding. Furthermore, designs attempted using AASHTO's uniform load method and AASHTO's single mode method were found to be equally unsatisfactory in achieving a uniform distribution of ductility demands along the bridge length. Therefore, to simplify the design procedure and to better distribute ductility demand along BRBs in a bridge having multiple simply supported spans, here, an

[1]Bridge Engineer, Kiewit, 1687 114th Ave SE Suite 210, Bellevue, WA 98004 (corresponding author). ORCID: https://orcid.org/0000-0001-6335-2060. Email: homerofe@buffalo.edu

[2]SUNY Distinguished Professor, Dept. of Civil Structural and Environmental Engineering, Univ. at Buffalo, Buffalo, NY 14260. ORCID: https://orcid.org/0000-0003-1170-468X. Email: bruneau@buffalo.edu

Note. This manuscript was submitted on June 1, 2023; approved on November 1, 2023; published online on January 4, 2024. Discussion period open until June 4, 2024; separate discussions must be submitted for individual papers. This paper is part of the ***Journal of Structural Engineering***, © ASCE, ISSN 0733-9445.

equivalent lateral force (ELF) design procedure is proposed; it has been developed based on the results from the optimum design approach based on NL-RHA described in Carrion-Cabrera and Bruneau (2022a).

Note that a first tentative ELF procedure developed based on limited results from NL-RHA was first attempted (Bruneau and Carrion-Cabrera 2020), but considering only a limited subset of design cases. Demands obtained from NL-RHA for bridges designed with this procedure were good; however, when larger ductilities or different BRB yield deformations were used, demands were subsequently found to be unacceptable. Therefore, here, that initial design procedure was improved by a broader and more complete set of response results from bridges designed with NL-RHA (Carrion-Cabrera and Bruneau 2022a). The process to develop the ELF procedure presented here is described on detail in the next subsections and is shown to be adequate to achieve the intended objective.

Bridges Archetype

The focus here is on regular straight simply-supported multi-span bridges having odd number of spans, implemented with BRBs in the longitudinal direction, and with spans supported by bidirectional sliding bearings. The bearings are assumed to have negligible lateral strength and to be supported on rigid abutments and elastic piers. This is consistent with the targeted seismic performance of keeping the substructure and superstructure elastic while BRBs behave inelastically, limiting maximum forces in the structure. BRBs can be implemented in bridges in the longitudinal direction in several different configurations, each resulting in different ductility demands. Carrion-Cabrera and Bruneau (2022b) recommended using the configuration where BRBs are connecting spans to piers and where BRBs connected to the same pier have the same properties. Note that for this configuration at least one of the two BRBs connected to the pier can reach the target ductility. Fig. 1 shows a sketch of the type of bridges studied here. Further research will consider different and more complex bridge archetypes and geometries, which are beyond the scope of this paper.

For this study, the values of parameters were set to cover a large range of possible bridges. The number of spans ranged from 3 to 11, the span mass was arbitrarily set equal to 175.55 Mg (1 kip s^2/in) since the controlling parameter is T_p defined by Eq. (1) representing the ratio span mass to pier stiffness (Carrion-Cabrera and Bruneau 2022a), the piers stiffness ranged from 1.76 kN/mm (10 kip/in) (representing a flexible pier) to 702.22 kN/mm (4,000 kip s/in) (representing a rigid pier), the ratio of the mass of the pier to the span mass was set equal to 0.1, and a base yield displacement of the BRB was set equal to 3.505 mm (0.138 in). Such yield displacement was represented by a BRB with an equivalent length equal of 2,032 mm (80 in), a length calculated to be adequate

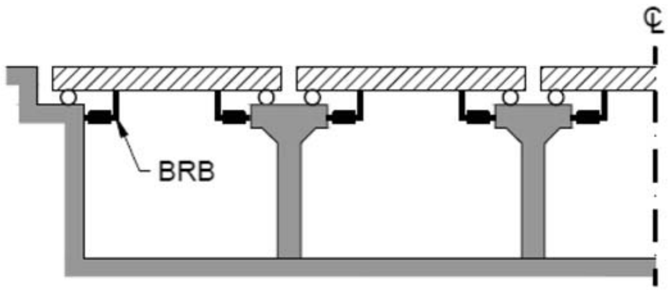

Fig. 1. Bridge with BRBs.

Table 1. Summary of parameters considered

Parameter	Values
Span mass	175.55 Mg (1 kip s^2/in)
Number of spans	3, 5, 7, 9, and 11
Pier stiffness range	1.76 to 702.22 kN/mm (10 to 4,000 kips/in)
BRB yield displacement	1.753, 3.505, 7.010 mm (0.069, 0.138, 0.276 in)
Target ductility	5 and 10
BRB equivalent length	2,032 mm (80 in)

to prevent low-cycle fatigue under annual thermal cycles (Wei and Bruneau 2016) for an arbitrary span length equal to 30.48 m (100 ft) and a Grade 50 steel, which has a yield strength equal to 345 MPa (50 ksi). Additionally, yield displacement values of 1.753 mm (0.069 in) and 7.01 mm (0.276 in) were also considered, representing a yield displacement larger and smaller than the base yield displacement. These yield displacements represent BRBs with equivalent lengths equal of 1,016 and 4,064 mm (40 and 160 in), still with a Grade50 steel. The target BRB displacement as expressed by the target BRB ductility (i.e., normalized by the BRB yielding displacement) were 5 and 10. Values for all these parameters are summarized in Table 1. A more detailed explanation of these parameters and how they were selected is presented in Carrion-Cabrera and Bruneau (2022a)

$$T_p = 2\pi\sqrt{\frac{m}{k}} \tag{1}$$

All bridges considered here were first designed using NL-RHA to effectively reach the target ductility in at least one BRB in each span along the bridge. This design was called the optimum design. The response of the bridge for this optimum design obtained from the NL-RHA was then used here to calibrate the proposed equivalent lateral force method. Selected NL-RHA results are presented in this paper for illustration purposes. Additional results are presented in detail in Carrion-Cabrera and Bruneau (2022a).

Equivalent Lateral Force Method Definition

The proposed ELF method considers seismic loads applied to the structure as equivalent lateral forces with a given distribution along the bridge length such as to generate the maximum deformation in all BRBs at the same time. This proposed procedure is similar in format to the ELF procedure in ASCE/SEI 7-16 (ASCE 2017), where the distribution of forces is obtained by the use of an equivalent mode shape where forces are distributed along the height of a building, with the mode shape expressed as function of the period of the structure. Analogous to what was done for buildings, the ELF procedure proposed and applicable to the bridges studied here is calibrated to capture the dynamic response of the bridge. Special emphasis is put on the equivalent mode shape that provides the distribution of forces along the bridge.

The equivalent mode shape is used because in a general case, none of the mode shapes of the structure can fulfill the requirement to generate the maximum deformation in all of the BRB, or even the maximum displacements along the structure, because the maximum deformations in each BRBs are reached at different times due to the combination of different modes and the nonlinearity of the structure's response. Therefore, if the objective is to have a single mode that would produce the same deformation (and yield deformation) in the BRBs that were observed from NL-RHA that reached the target ductility, then a special mode shape is required—one that would have to be defined for this purpose. This special mode shape is called here an equivalent mode shape. Using this mode shape, the deformation in BRBs can be written as:

$$\{\boldsymbol{\Delta}_{\mathbf{BRB}}\} = [\mathbf{T}]\{\boldsymbol{y}\} = [\mathbf{T}][\boldsymbol{K}]^{-1}[\boldsymbol{M}]\{\boldsymbol{\phi}\}\boldsymbol{Sa}(\boldsymbol{T}_1) \tag{2}$$

where $\{\mathbf{y}\}$, $[\boldsymbol{T}]$, $\{\boldsymbol{\Delta}_{\mathbf{BRB}}\}$, $[\boldsymbol{K}]$, $[\boldsymbol{M}]$, $\{\boldsymbol{\phi}\}$, and $S_a(T_1)$ are respectively: the vector of displacement of the structure, a topological matrix used to calculate the deformations in BRBs, the vector of deformation of BRBs, the stiffness matrix of the structure, the mass matrix, the mode vector, and the pseudo acceleration at the fundamental period of the structure.

For the application studied here, the equivalent mode (that belongs to the ϕ vector space) is defined as the combination of several linear independent vectors (basis vectors of the ϕ vector space), similar to the definition of Ritz vectors modes; however, here, they are combined to form the equivalent mode shape. Thus, the equivalent mode shape is defined as:

$$\boldsymbol{\phi} = a_1\boldsymbol{\phi}_1^* + \cdots + a_{n-1}\boldsymbol{\phi}_{\boldsymbol{n}-1}^* + a_n \cdot \boldsymbol{\phi}_{\boldsymbol{n}}^* \tag{3}$$

where a_i are constants, and $\boldsymbol{\phi}_{\boldsymbol{i}}^*$ is the ith vector of the basis of the ϕ vector space. Each vector in the basis is defined such that the combined mode varies linearly from span to span (e.g., the mode shape value at the mass at the top of the piers is an average of the mode shape value for each adjacent span). As a result, the mode shape is linear piecewise with nodes at the mass spans.

The characteristic of each vector in the basis is explained with the example of a 3-span bridge. This bridge has 6 BRBS but due to symmetry, the analysis reduces to 3 BRBs (i.e., those in one half of the bridge). From those 3 BRB, two of them are connected to the same pier, and therefore, based on the constraint that all BRBs connected at the same pier have the same cross-section area, only one of those two will reach the target ductility. The problem thus reduces to the analysis of 2 BRBs that are intended to reach the target ductility. Since the 3-span bridge is symmetric, only two vectors of the basis are required. Each vector component considers a value equal to 1 at the span mass and 0.5 at adjacent mass piers; written in matrix format it is:

$$\boldsymbol{\phi} = \begin{bmatrix} 1 & 0 \\ 0.5 & 0.5 \\ 0 & 1 \\ 0.5 & 0.5 \\ 1 & 0 \end{bmatrix} \begin{Bmatrix} a_1 \\ a_2 \end{Bmatrix} \tag{4}$$

The values equal to 0.5 are used to create a linear interpolation between the equivalent mode value at each mass span and to consider the influence of the mass lumped at the top of the pier. Substituting Eq. (4) in Eq. (3), the values of a_1 and a_2 can be obtained to reach the yield deformation in each BRBs corresponding to the target ductility. After obtaining the values for a_1 and a_2, the mode was normalized by a_2 (as typically done with mode shapes). Note that it is beneficial to have a mode shape with maximum deformation at the center of the bridge as a normalization process to compare mode shapes between different bridges.

Considering that the bridge is analyzed in the longitudinal direction, the length of the span is not important (due to the relatively high axial stiffness of the spans compared to that of the BRBs). Therefore, the bridge is represented by lumped masses in series. The position of each mass is expressed by its normalized position, x. The normalized value transforms any bridge considered into a bridge with a normalized length equal to 2. The center of this bridge is considered the origin of the system. As a result, its ends are at -1 and 1. The location of each lumped mass representing a span, m_i, is also normalized as follows:

$$x = \frac{(N_{\text{span}}+1)/2 - i}{(N_{\text{span}}-1)/2} = \frac{N_{\text{span}}+1-2i}{N_{\text{span}}-1} = 1 - 2\frac{i-1}{N_{\text{span}}-1} \tag{5}$$

where i is the number of the span counting from the left abutment. With the mode shape defined by Eq. (3), the equivalent lateral force is calculated with Eq. (6) where R is a seismic reduction factor and W is the total weight of the bridge

$$F_i = \frac{W\,Sa(T)}{R}\frac{m_i\phi(x_i)}{\sum_{j=1}^{n} m_j\phi(x_j)} \tag{6}$$

The proposed design procedure requires to calculate the period of the structure, to calculate the mode shape and to define the reduction factor. All these parameters were calculated using equations fitted to the result obtained for all bridges designed with NL-RHA procedure, and defined as described as follows. Note that the design procedure described here is the one retained after several other different options were considered but found to be less successful.

Prediction of the Period of the Structure

In this section, the fundamental period obtained for bridges designed using NL-RHA is defined by a simple equation obtained by fitting a curve to the results. Here, the period of a single span analyzed as a SDOF system with yield deformation equal to the BRB yield deformation and designed to reach a set target ductility is the smallest period, $T_{\min}$, that the structure can have to reach the target ductility (i.e., it corresponds to a bridge with rigid piers). The period obtained from the NL-RHA procedures for bridges having the stiffest piers considered (approaching infinitely stiff piers) and for their corresponding SDOF systems are listed in Table 2. Note that in all cases the period obtained with the SDOF system is smaller than the period obtained from optimization, but the difference is not significant (max 0.03 s). Therefore, for the following calculations, the period obtained from the SDOF was used for simplicity and for the benefit of its physical meaning.

The fundamental period of bridges, T_1, designed with the NL-RHA optimization procedure (Carrion-Cabrera and Bruneau 2022a) ranges from 0.13 to 1.90s. Also, it was observed that periods expressed as the ratio represented by Eq. (7) exhibit a common trend if they are plotted against the ratio $T_p/T_{\min}$, as shown in Fig. 2. Eq. (8) was developed to capture the trend in behavior (without being an exact best-fit), referred to hereafter as the fitted values. The comparison between result for all the spans and from Eq. (8) is shown in the figure. Comparing data and the fitted values, depending on the BRB yield deformation, the period of the bridge [per Eq. (8)] seems have an upper limit (which incidentally increases as the BRB yield deformation increases, although this is not shown in the following figures). This limit is not captured with Eq. (8), but it is indirectly corrected by the R value described later when the equation of the R value is defined

Table 2. Minimum period of the structure (in s)

	$\mu = 5$		$\mu = 10$	
Yield deformation (mm) (in)	SDOF	Bridge with the stiffest pier considered	SDOF	Bridge with the stiffest pier considered
1.753 (0.069)	0.13	0.16	0.16	0.19
3.505 (0.138)	0.20	0.23	0.28	0.29
7.010 (0.276)	0.34	0.35	0.65	0.67

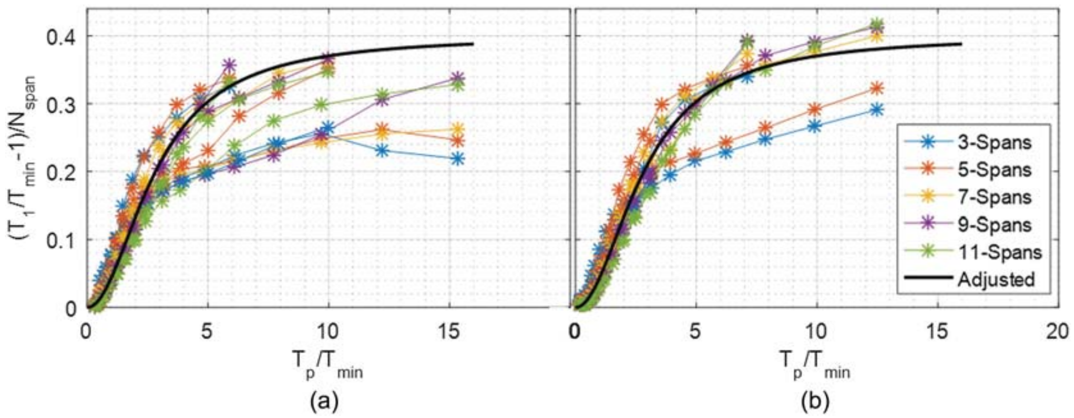

Fig. 2. Fitted equation for the fundamental period of the structure: (a) $\mu = 5$; and (b) $\mu = 10$. Note: 1 in = 25.4 mm.

$$\left(\frac{T_1}{T_{\min}} - 1\right)\frac{1}{N_{\text{span}}} \tag{7}$$

$$\left(\frac{T_1}{T_{\min}} - 1\right)\frac{1}{N_{\text{span}}} = 0.4\left[1 - \frac{8}{\left(\frac{T_p}{T_{\min}}\right)^2 + 8}\right] \tag{8}$$

Equivalent Mode Shape

As a parallel process, the equivalent mode shape of the structure was obtained for all the bridges designed with the NL-RHA optimization procedure (i.e., the a_i constants in Eq. (3) were calculated), and these mode shapes are shown in Figs. 3 and 4 in dashed lines. Note that for the stiffest pier considered here ($T_p = 0.1$ s), the equivalent mode shapes are not straight lines, meaning that the behavior of

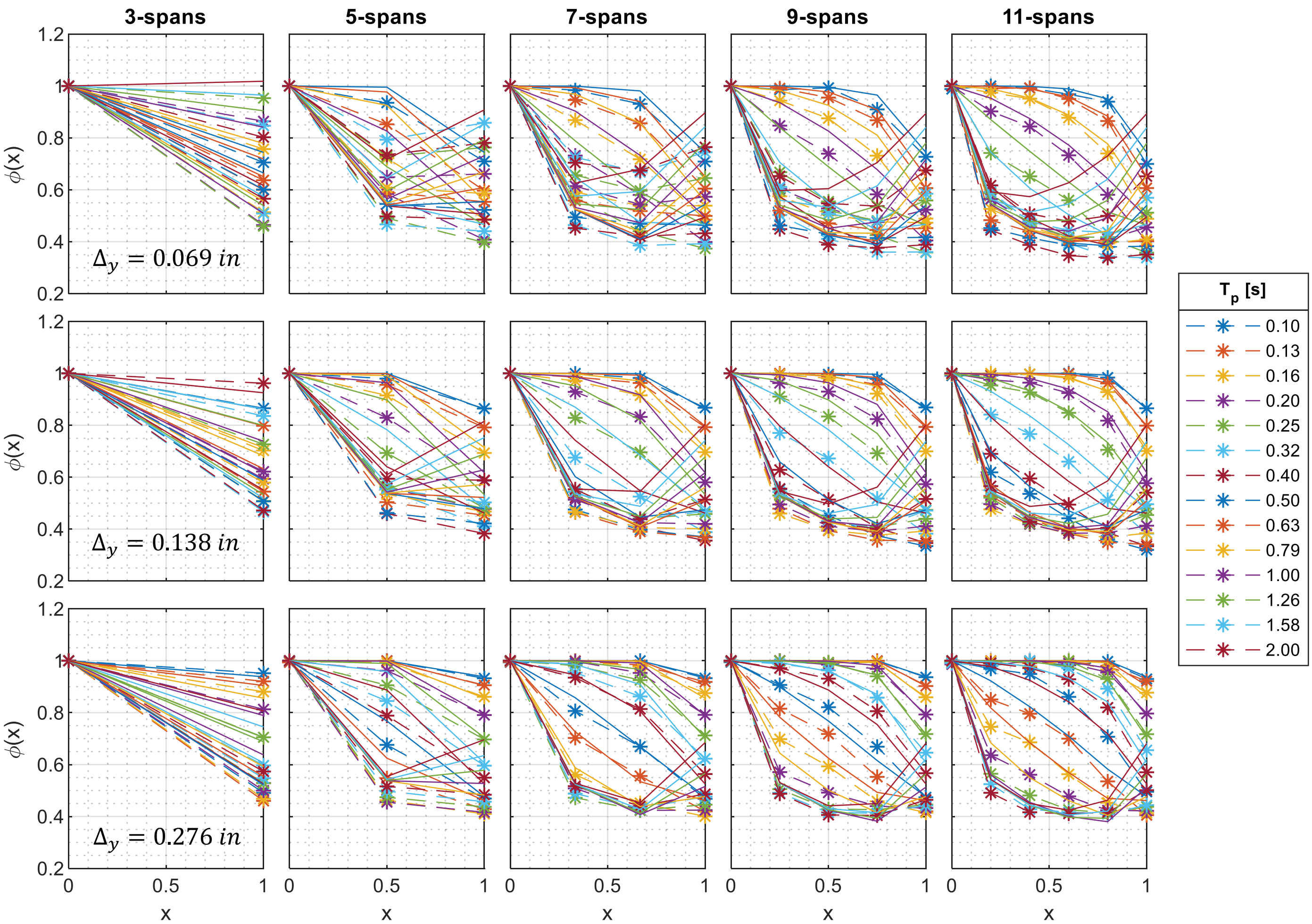

Fig. 3. Equivalent mode shapes for bridges with different number of spans and different T_p and a target ductility $\mu = 5$. Note: 1 in = 25.4 mm.

J. Struct. Eng., 2024, 150(3): 04024003

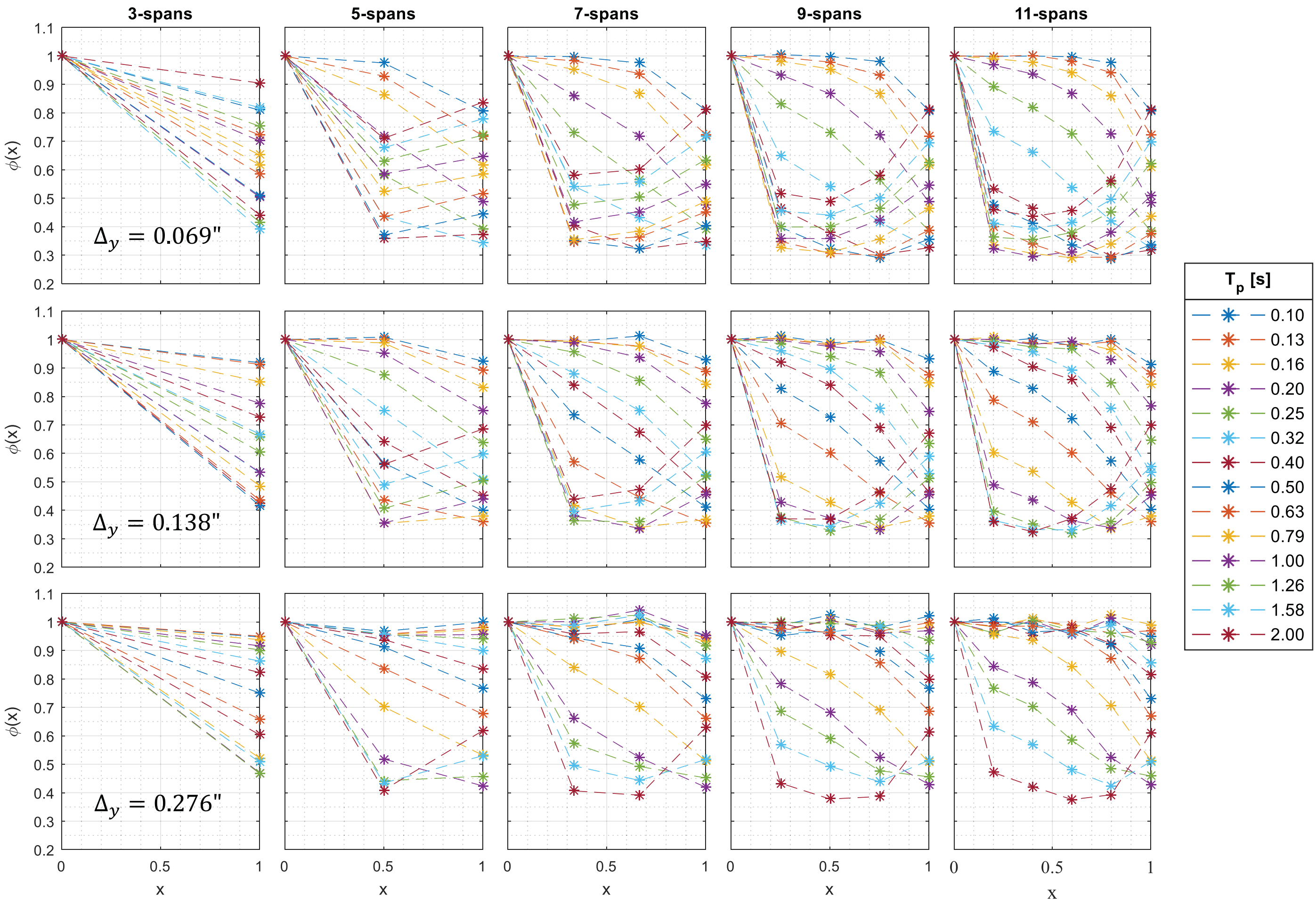

Fig. 4. Equivalent mode shapes for bridges with different number of spans and different T_p and a target ductility $\mu = 10$. Note: 1 in = 25.4 mm.

the spans are not totally decoupled from each other (as would be the case for bridges having extremely rigid piers). The exception here being with the behavior of the spans close to the center of the bridges, which seems to be decoupled from the behavior of adjacent spans, similarly to what would be observed for independent SDOF systems, and this is more evident in the equivalent mode shapes for the 11-span bridges having the largest BRB yield deformation. Note that for the bridges with the largest BRB yield deformation, the equivalent mode shape is almost a straight line, independently of the number of spans. However, for the smallest BRB yield deformation, this similarity to a straight line is lost, which indicates that the pier stiffness for these bridges is not rigid enough to make each span behaves as an independent SDOF system. For that reason, the period of the SDOF, showed in Table 2, is smaller than the period obtained for the bridge with highest pier stiffness considered.

Also note that the equivalent mode shape has a concave downward shape when the pier is relatively rigid, but then reduces to become a straight line and later transition to become convex for flexible piers. The limit period, or the T_p value when the equivalent mode shape is practically a straight line was not constant for all the bridges under study, but instead varied based on the number of spans.

Based on the previous analysis, the function to be selected to represent these equivalent mode shapes should be able to change its curvature as function of the period of the pier. To capture this phenomenon, the mode shape was redefined in Eq. (9) to be the sum of two functions defined by Eq. (10), where k_1 and k_2 change with the period of the structure; x ranges from -1 to 1; and a, b, and c are constants to be determined based on the mode shape results. From the equivalent mode shapes, shown in Figs. 3 and 4, it is also observed that the minimum value of the equivalent mode shape reduces as the target ductility increases. The minimum values are approximately 0.35 and 0.30 for a target ductility equal to 5 and 10, respectively. The maximum value of the equivalent mode shape is always equal to one when $x = 0$ (at the center of the bridge). Based on Eq. (10), the minimum value of the equivalent mode shape is at $x = 1$ and is given by the constant a when k tends to infinity. The maximum value of the function is at $x = 0$, and is equal to $a + b$. Solving these equations, the value of a and b are determined. In the case of c, it must have a value more than 1 to capture the concave curvature of mode shapes when piers are relatively rigid; a value of 1.1 was found to be suitable for all cases. The value of all the constants in Eq. (10) are given in Table 3. The parameter k_1 and k_2 were obtained from curve fitting by trial and error

$$\phi(x, k_1, k_2) = 1 + y(x, k_1) - y(x, k_2) \tag{9}$$

Table 3. Constant values for equation of the mode shape

Target ductility	a	b	c
5	0.35	0.65	1.1
10	0.30	0.70	1.1

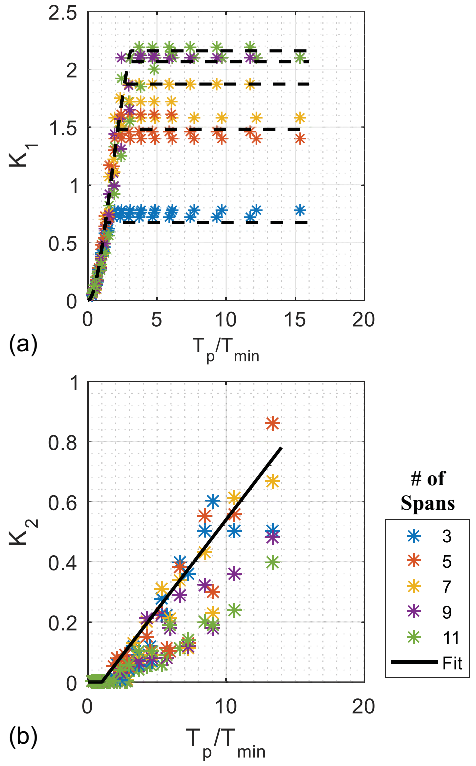

Fig. 5. Fitted equation for bridges with $\mu = 5$ for: (a) k_1; and (b) k_2.

$$y(x, k) = \mathrm{a} + \mathrm{b} \cdot \left(1 - \frac{|x|^{\frac{1}{k}}}{\mathrm{c}}\right)^k \qquad (10)$$

It was observed that the values of k_1 is related to the ratio of $T_p/T_{\min}$. Values obtained by curve fitting of the mode shape are shown in Figs. 5(a) and 6(a). From the figures, it is also observed that k_1 has an upper limit related to the number of spans, which increases as the number of spans increases. The maximum values of k_1 for a given number of spans and different yield deformations are close to each other but are different from values obtained for bridges having different target ductility. Therefore, data was divided according to the target ductility and analyzed independently. Two functions were used to represent k_1 for results for each target ductility: one to represent the common trend and a second to represent the upper limit values. The values of k_1 for a target ductility equal to 5 and 10 were fitted with Eqs. (11) and (12), respectively, where the right side of the equations represents the upper limit. Note that the upper limit in the equations for k_1 varies only as a function of the target ductility and the number of spans (right side of the equation). The best fit values are shown in Figs. 5(a) and 6(a), and the values of $T_p/T_{\min}$ for the maximum k_1 are listed in Table 4.

Values of k_2 were also related to the ratio $T_p/T_{\min}$. Values obtained by curve fitting of the mode shape are shown in Figs. 5(b) and 6(b). From the figure, it is observed that k_2 does not have an upper limit, but instead has a lower limit equal to zero for values of $T_p/T_{\min} \leq 1$. For the case of $\mu = 5$, k_2 was fitted with Eq. (13). This fit was done to make k_2 approximately equivalent to an upper bound for all the data (i.e., for all the results obtained) since a large value of k_2 will increase the area in BRBs connected to the abutment, which typically reduces the possibility of concentration of BRB ductility demand there as was observed before. For the bridges with target ductility equal to 10, the same equation, Eq. (13), was found to be valid

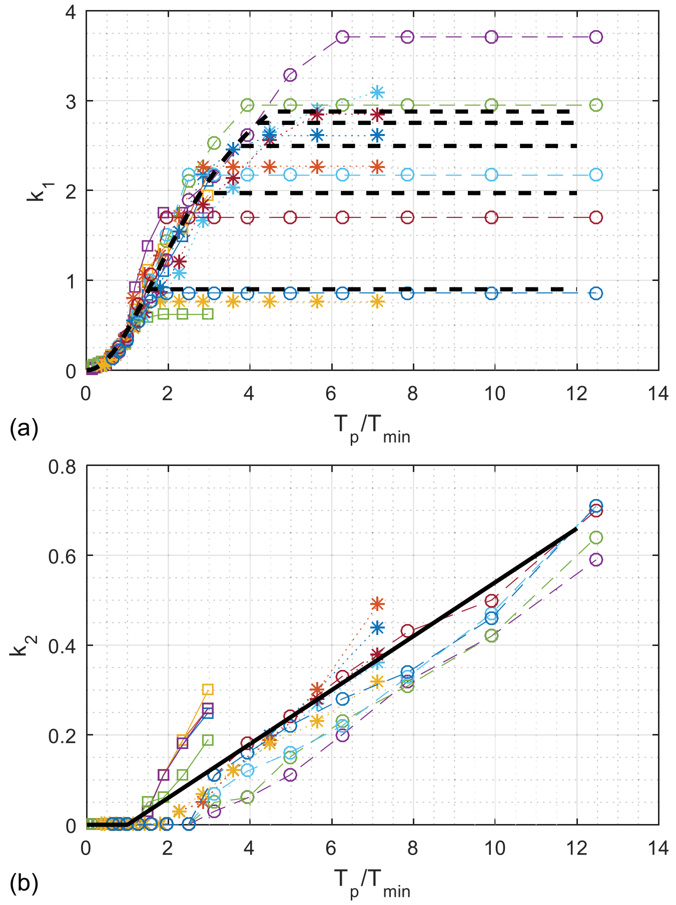

Fig. 6. Fitted equation for bridges with $\mu = 10$ for: (a) k_1; and (b) k_2.

Table 4. $T_p/T_{\min}$ for maximum k_1

Target ductility	Number of spans				
	3	5	7	9	11
5	1.27	2.17	2.65	2.92	3.06
10	1.52	2.78	3.64	4.20	4.53

$$k_1 = 4\left[1 - \frac{8}{\left(\frac{T_p}{T_{\min}}\right)^2 + 8}\right] \leq 2.25(1 - 0.7^{N_{\mathrm{mas}}-2}) \qquad (11)$$

$$k_1 = 4\left[1 - \frac{8}{\left(\frac{T_p}{T_{\min}}\right)^2 + 8}\right] < 3(1 - 0.7^{N_{\mathrm{mas}}-2}) \qquad (12)$$

$$k_2 = 0.06\left(\frac{T_p}{T_{\min}} - 1\right) > 0 \qquad (13)$$

With the fitted equations, the mode shapes were calculated for bridges with target ductility equal to 5 and 10, and are respectively shown in Figs. 3 and 7 as continuous lines. In these figures, values are relatively well represented by the best-fit functions. Fig. 8, shows another comparison between the predicted values of the mode shape at different x locations and those obtained from the NL-RHA designs for different locations in the bridge. It is observed that these predicted values visually appear to be a good match considering the simplicity of the preceding best-fit method.

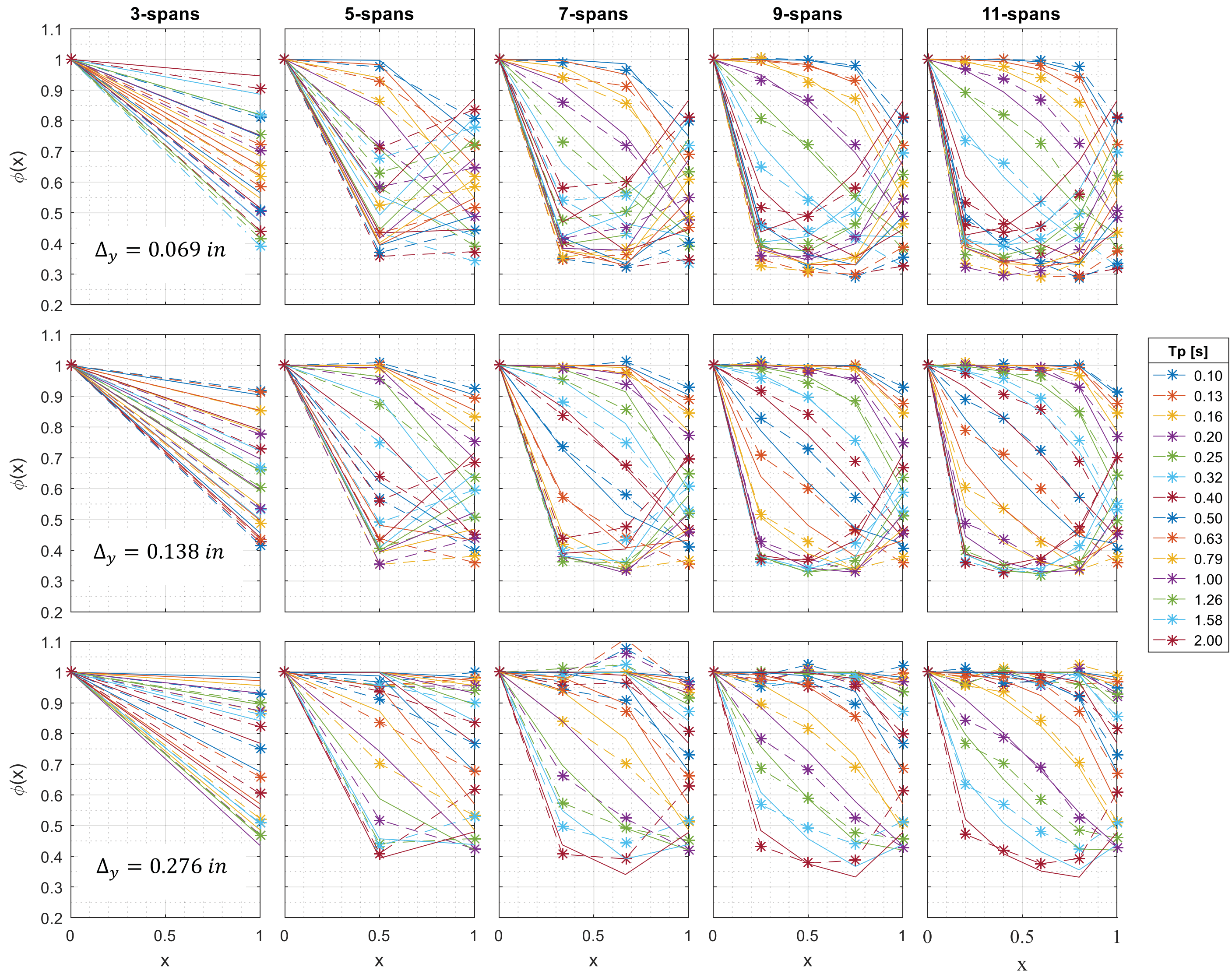

Fig. 7. Fitted equivalent mode shapes for $\mu = 10$. Note: 1 in = 25.4 mm.

Reduction Factor

The fitted mode shape and period equations defined previously were used to calculate the reduction factor, R, to be used in the ELF procedure. The reduction factor is used in Eq. (6), where Sa(T) is calculated at the fundamental period of the structure, T_1, as approximated by Eq. (8) (this selection result in conservative R values compared with the case where the period from NL-RHA is used). Note that $Sa(T_1)$ is the pseudo acceleration that is obtained from the design spectrum, $\phi(x)$ is the equivalent mode shape calculated with Eqs. (9)–(13), and R is the unknown value to be determined. The lateral forces, F_i, are also unknown; however, the expected effects of these loads are known, which is to reach the yielding deformation on the BRBs of interest (namely, the ones connected to the abutment and one of the BRBs connect to each pier). Mathematically, the deformation in all BRBs can be expressed as:

$$\{\mathbf{\Delta_{BRB}}\} = [\boldsymbol{T}]\{\boldsymbol{y}\} = [\boldsymbol{T}][\boldsymbol{K}]^{-1}\{\boldsymbol{F_i}\} \tag{14}$$

where $[\boldsymbol{K}]$ is the stiffness matrix calculated from the bridge designed with NL-RHA.

The vector $\{\mathbf{\Delta_{BRB}}\}$ contains the BRB deformation from all BRBs. For this elastic based analysis, from the two BRBs connected to the pier, it is considered that the BRB that reaches the target ductility is the one with the largest deformation. From the vector $\{\mathbf{\Delta_{BRB}}\}$, a subset is defined as $\{\mathbf{\Delta_{BRB_{Max}}}\}$ that contains the deformations of all BRBs expected to reach the target ductility demand. The minimum value of this subset was selected to calculate the reduction factor. The reduction factor is obtained from:

$$R = \frac{\min\{\mathbf{\Delta_{BRB_{Max}}}\}}{\Delta_y} \tag{15}$$

The R value calculated with this minimum value of the subset results in the minimum reduced seismic lateral force on the system that makes all BRBs of the subset reach at least their yielding deformation based on an elastic analysis of the bridge with the optimum design, which is conservative.

Reduction factors resulting from Eq. (15) considering different BRB yield deformations, different pier stiffnesses, and different number of spans are shown in Fig. 9. Note that only when piers are infinitely stiff, and for the same yield deformation and target ductility, reduction factor tends to be the same for all bridges. This is

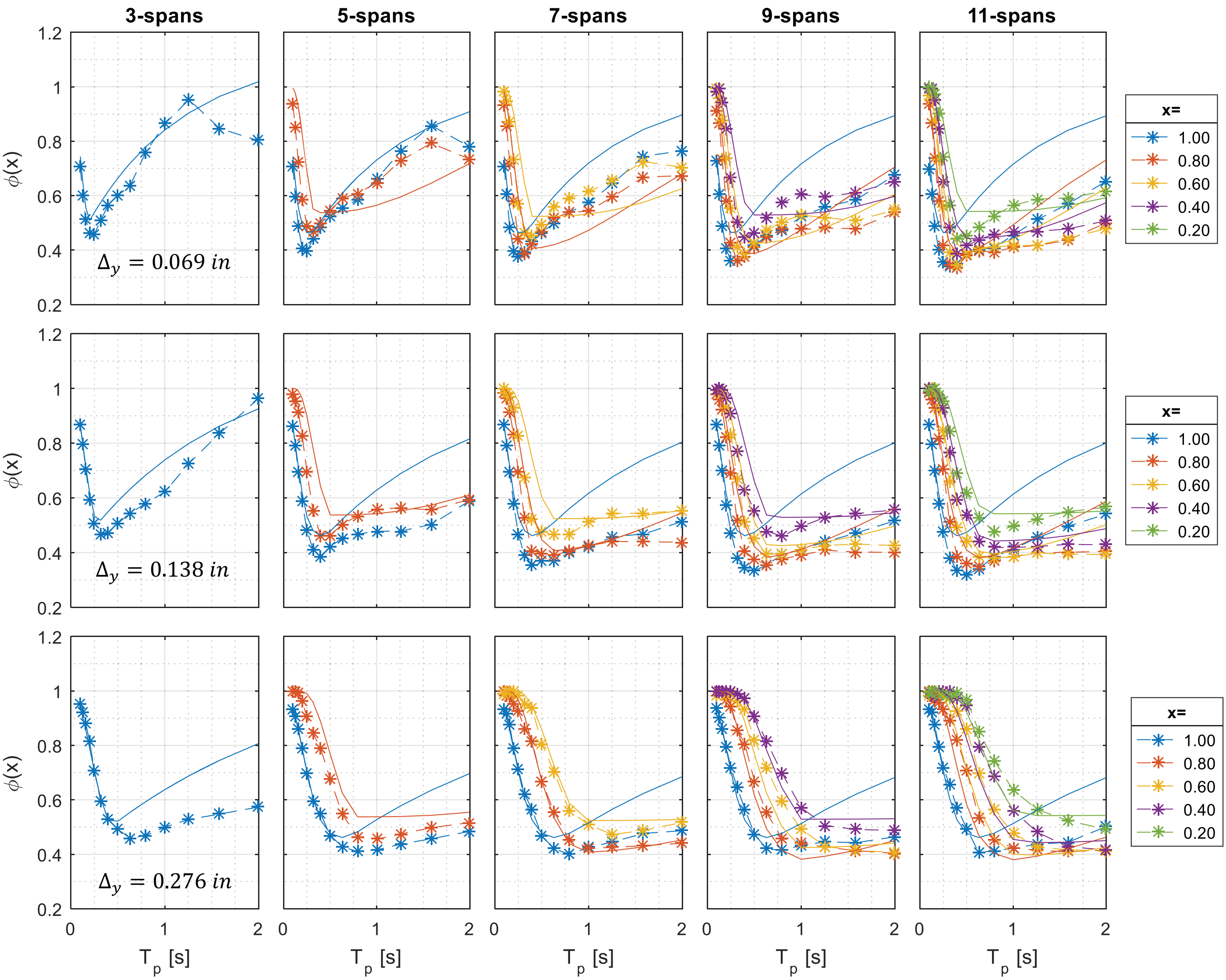

Fig. 8. Equivalent mode shapes values at different x locations versus T_p for $\mu = 5$. Note: 1 in = 25.4 mm.

because each span behaves similarly to a SDOF system in that case. However, when the pier stiffness reduces, and therefore the period of the pier increases, the reduction factor changes depending the number of spans. A conservative value to use for design would be the one that uses the lower envelope of all the curves, resulting in the smallest reduction factor.

As a result, for the case of an infinitely stiff pier and based on results presented in Carrion-Cabrera and Bruneau (2022b), when spans can be modeled as SDOF, the reduction factor can be obtained as:

$$1.0 \leq \alpha_\mu = 0.06\mu_{\text{SDOF}} + 0.7 \leq 1.3 \tag{16}$$

$$R(T_1) = \begin{cases} \left(\dfrac{\mu_{\text{SDOF}}}{\alpha_\mu} - 1\right)\dfrac{T_1}{1.25T_s} + 1 & if\ T_1 < 1.25T_s \\ \dfrac{\mu_{\text{SDOF}}}{\alpha_\mu} & \text{otherwise} \end{cases} \tag{17}$$

where α_μ is a modification factor valid for ductility larger than 5 and less than 10.

However, when piers are flexible, the reduction factor changes as the period of the pier changes, either reducing or increasing. In comparison, in a SDOF system, when the period of the system increases, the reduction factor typically increases. As such, a behavior similar to SDOF systems is not observed in this case. When the substructure stiffness reduces, the period of the pier and the structure increases; however, the reduction factor still reduces. For a target ductility equal to 5, it is observed that in all cases the reduction factor converges to a value of 2.5. For the case of target ductility equal to 10, the reduction factor converges to a value of 4 when piers are flexible. Therefore, Eqs. (18) and (19) are proposed here to calculate the reduction factor to be used with the ELF procedure. This calculated reduction factor is independent of the number of spans and is shown as a thick black line in Fig. 9

$$R(T_1) = \begin{cases} \left(\dfrac{\mu_{\text{SDOF}}}{\alpha_\mu \gamma_\mu} - 1\right)\dfrac{T_1}{1.25T_s} + 1 & if\ T_1 < 1.25T_s \\ \dfrac{\mu_{\text{SDOF}}}{\alpha_\mu \gamma_\mu} & \text{otherwise} \end{cases} \tag{18}$$

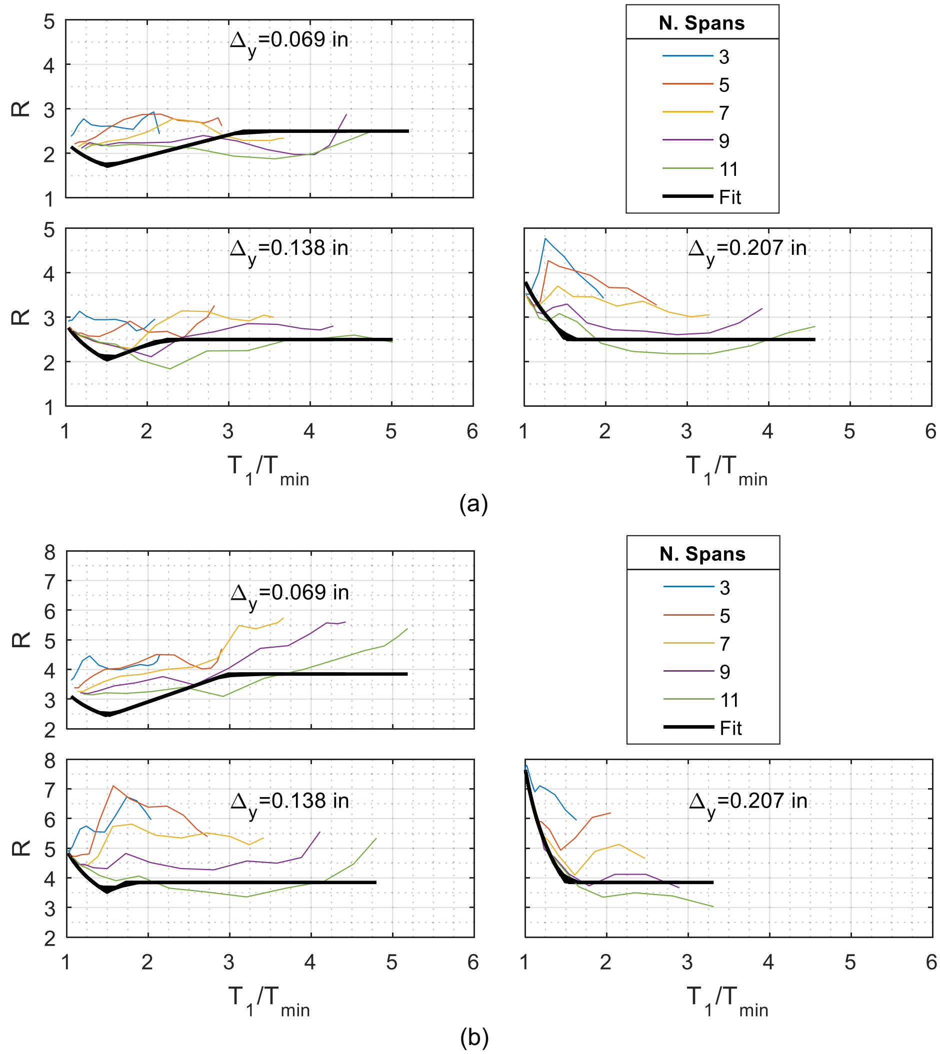

Fig. 9. Reduction factor for equivalent lateral force method for: (a) $\mu = 5$; and (b) $\mu = 10$. Note: 1 in = 25.4 mm.

$$\gamma_\mu = 1 + 2\left(\frac{T_1}{T_{\min}} - 1\right) \leq 2 \tag{19}$$

Using Eq. (8) to calculate the factor $(T_1/T_{\min} - 1)$ of the structure, the final reduction factor was calculated with Eq. (18) and is shown in Fig. 10 with asterisks.

Demands in Bridges Designed with the Proposed Procedure

To verify the adequacy of the proposed ELF design procedure using the approximated reduction factors described previously, BRBs were designed for 420 bridges having (14 different stiffness, 3 different yield deformation, 5 different number of spans, and 2 targets mean ductility) and the BRB ductility demand was obtained with NL-RHA. Results are shown in Figs. 11–15. Fig. 11 shows the resulting mean BRB ductility demand. Note that ductility demand does not exceed the target ductility for most of the bridges, except few cases and for some values of T_p. Moreover, demands are relatively well balanced in all BRBs and are not concentrated in only a few BRBs [contrary to what was observed in bridges designed with RSA (Carrion-Cabrera and Bruneau 2022b)]. Fig. 12 shows the 90th percentile of the BRB ductility demands. In most of the bridges, demand in BRBs are less than twice the target ductility, even for some of the bridges that showed mean ductility demand larger than the target ductility. For this upper limit (90th percentile), the worst case observed is in 11-span bridges with BRBs having short yield deformations. Recall, that the upper limit used here is a measure that emphasizes that only in 10% of the cases, the BRBs experience demands larger than those used during their qualification testing, and that it does not necessarily represent failure of the BRBs (because AISC-341 requires BRBs to be subjected to a qualification testing protocol up to at least twice their design displacement).

Fig. 13 shows the maximum mean and maximum 90th percentile of the BRB fatigue index [calculated following Li et al. (2022)] in a bridge, showing that the mean in most of the cases is less than 12% of its predicted fatigue life, meaning that even after an earthquake, the BRBs would not need to be replaced. For bridges where the 90th percentile of ductility demand is larger than twice the target ductility, in the worst case, the 90th percentile of the fatigue damage is less than 50% of its predicted fatigue life. Just for comparison, for the extreme case that could be considered an outlier, the worst fatigue damage obtained in one BRB is less than 80% of its predicted fatigue life, and this worst case was observed in only one bridge.

The drift displacement demands of the piers was also studied. The mean displacement demands in pier were normalized by the

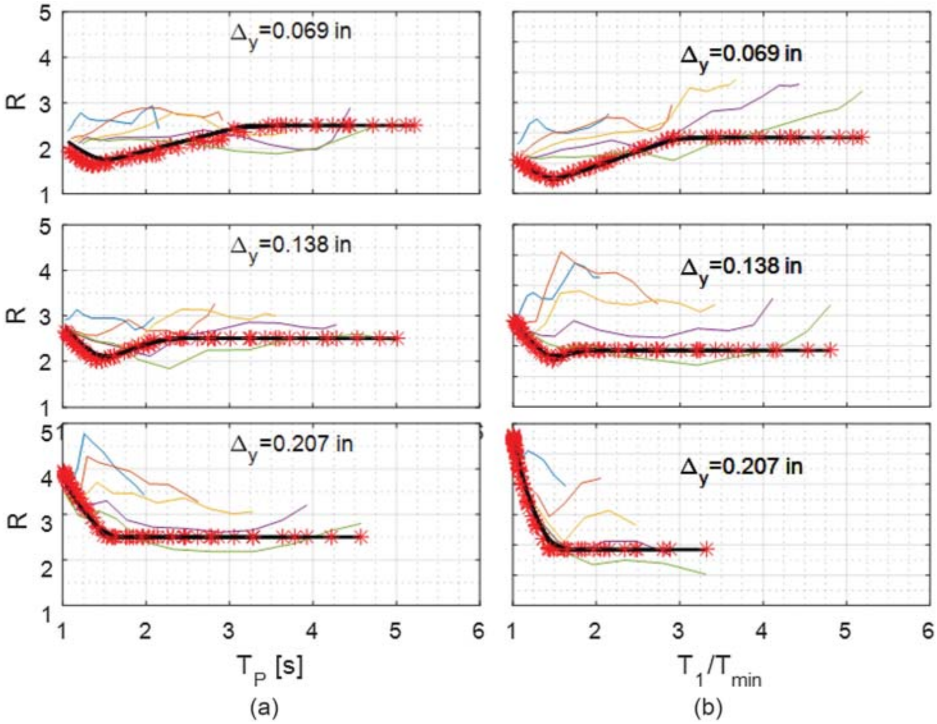

Fig. 10. Calculated reduction factor R: (a) $\mu = 5$; and (b) $\mu = 10$. Note: 1 in = 25.4 mm.

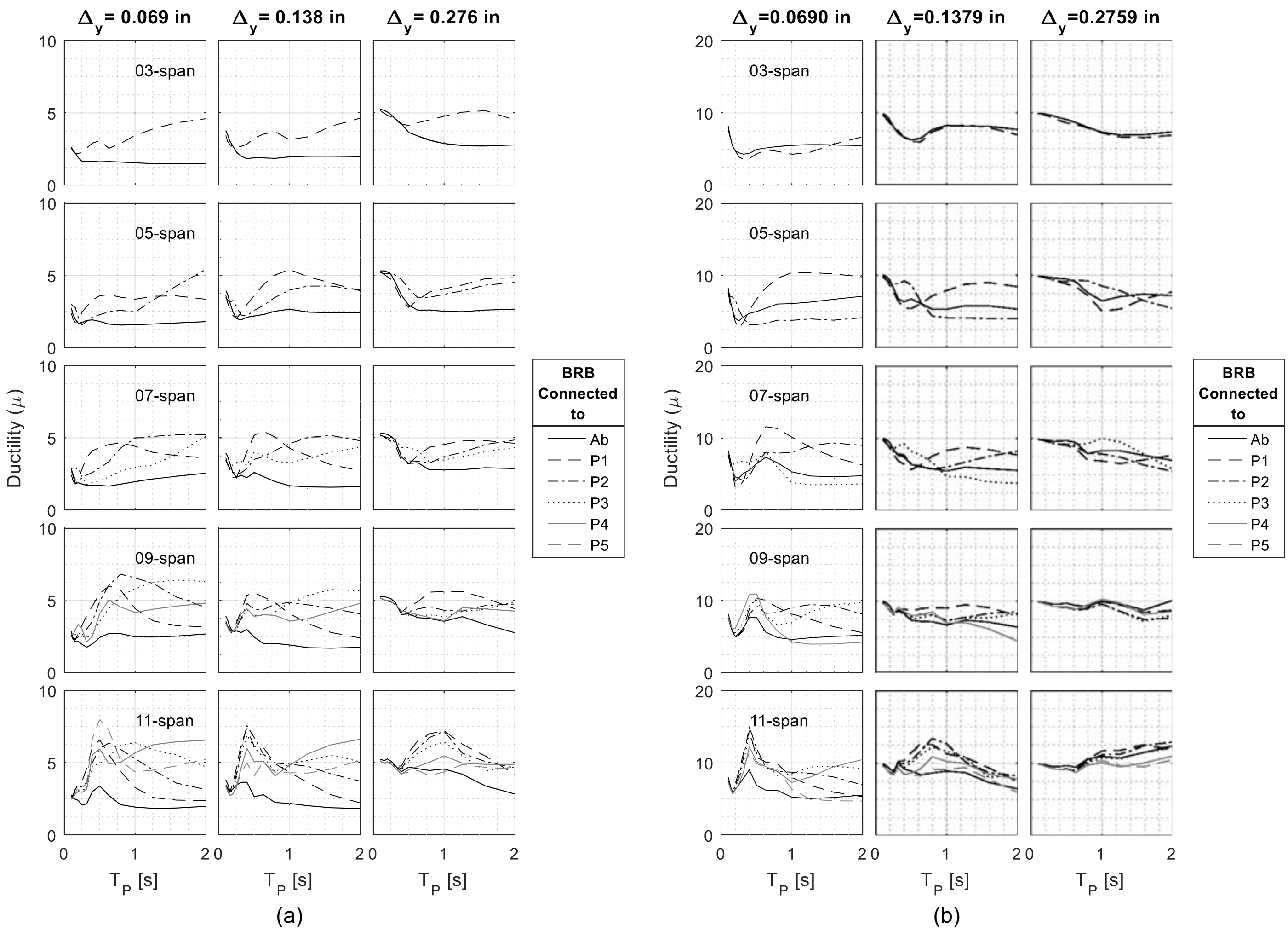

Fig. 11. Mean ductility demand: (a) $\mu = 5$; and (b) $\mu = 10$. Note: 1 in = 25.4 mm.

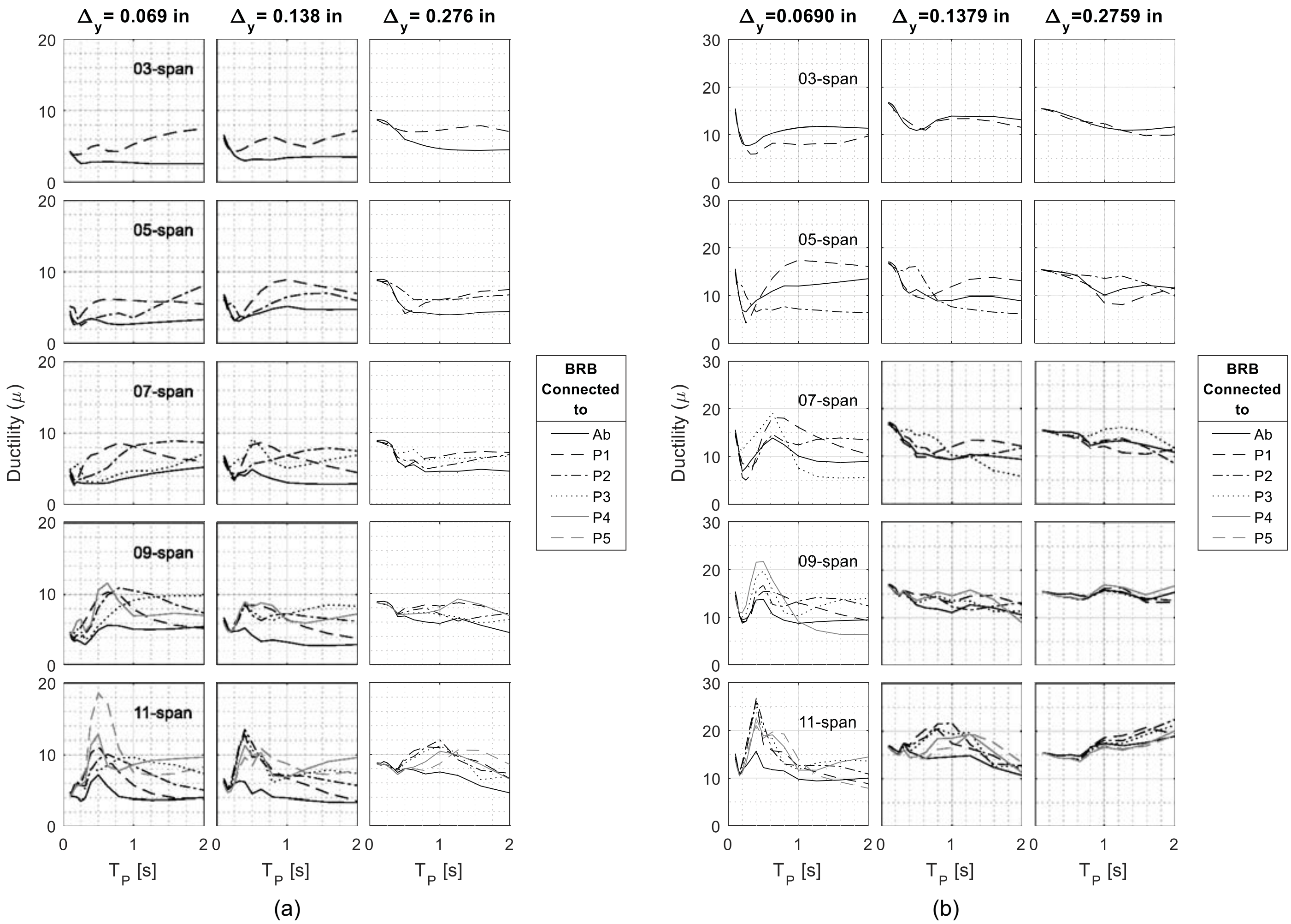

Fig. 12. 90th percentile of ductility demand: (a) $\mu = 5$; and (b) $\mu = 10$. Note: 1 in = 25.4 mm.

BRB yield deformation and were compared with the elastic displacement demand of one pier acting as a cantilever with its tributary mass lumped at the free end and having a period T_p (which represents the pier of benchmark bridges that have the span rigidly connected to the pier at one of its ends and free to move at the other, with its displacement demand also equal to the spectral displacement at the period T_p). Fig. 14 shows that mean displacements demand is always smaller than the elastic displacement of the pier of the benchmark bridge (labeled as EL. SDOF in the figure). The displacement demand for the first piers is the smallest of all the piers. For piers closer to the center of the bridge, this demand increases.

The displacement in expansion joints were also calculated and expressed as a normalized value with respect to the BRB yield displacement. In the case of 90th percentile of demands, shown in Fig. 15, it is observed that joint demands generally do not exceed twice the BRB target deformation. The exception to that observation is for cases with the smallest BRB yield deformation and with a target ductility equal to 5, which is not a problem since displacement demands are quite small in these cases; for example, for a ductility demand of 20, it would correspond to $20 \times 0.0690 = 1.38$," which can be accommodated by conventional expansion joints.

Finally, although not presented here, preliminary results indicate that the design procedure is sufficiently robust to give satisfactory results for irregular bridges, even though it was derived for regular bridges. In that sense, it is not that different from the ELF procedure for buildings, but more comprehensive future research is needed to establish the range of mass and stiffness variations that allows irregular bridges to be reliably designed by this proposed procedure.

General Design Procedure for Ductilities between 5 and 10

Based on the design procedure obtained previously for target ductilities equal to 5 and 10, it is assumed that results for intermediate values of target ductilities could be achieved by linear interpolation. This linear interpolation affects only to the approximation of the mode shape and k_1, and they were modified to Eqs. (20) and (21), respectively. Both equations introduce the target ductility demands, μ_{obj}, as a variable

$$y(x,k) = 1.0 - \left(0.60 + \frac{u_{\text{obj}}}{100}\right)\left[1 - \left(1 - \frac{|x|^{\frac{1}{k}}}{1.1}\right)^{k}\right] \quad (20)$$

$$k_1 = 4\left[1 - \frac{8}{\left(\frac{T_p}{T_{\min}}\right)^2 + 8}\right] \leq 1.5\left(1 + \frac{\mu_{\text{obj}}}{10}\right)(1 - 0.7^{N_{\text{mas}}-2}) \quad (21)$$

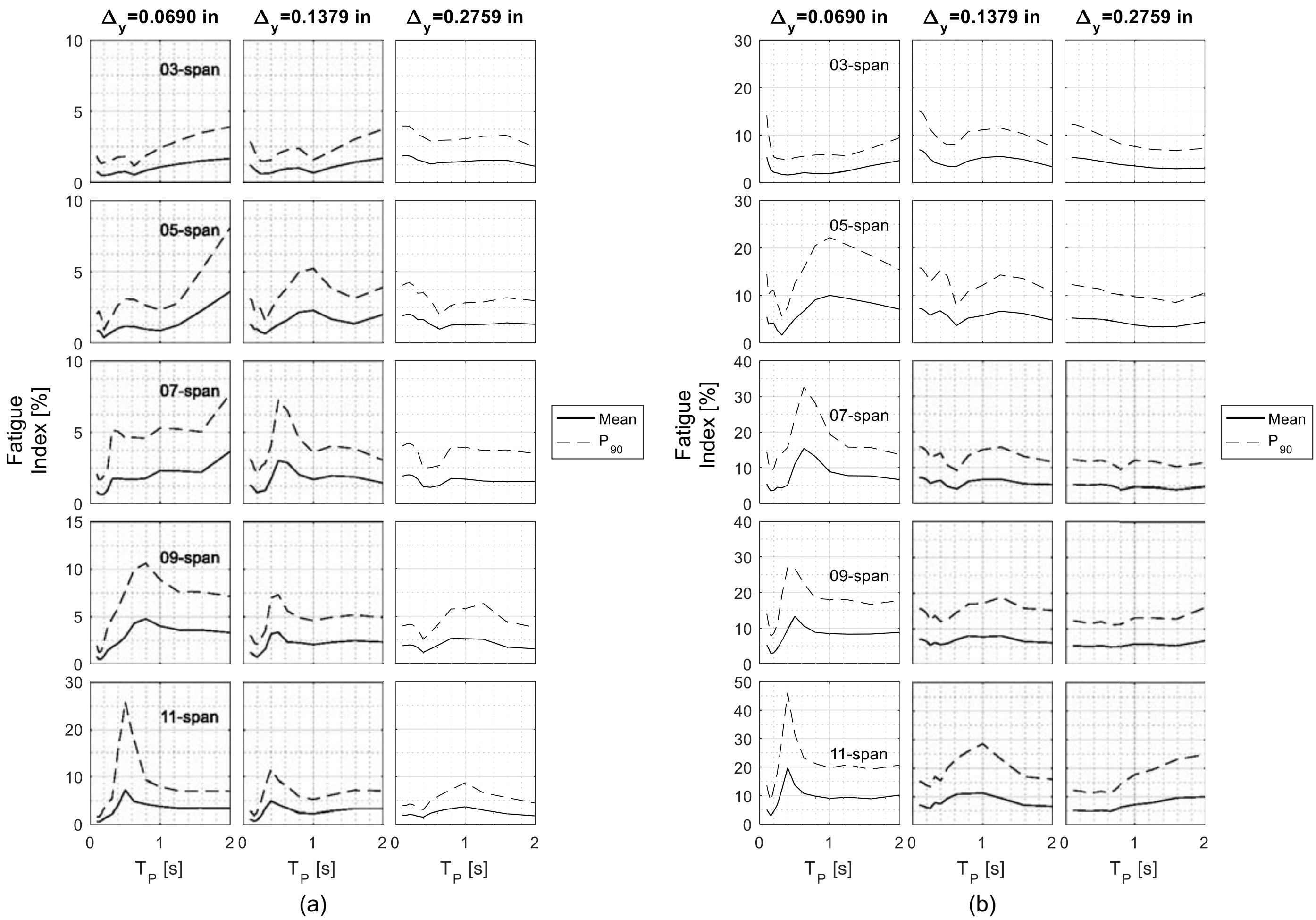

Fig. 13. Maximum mean fatigue and maximum 90th percentile of fatigue: (a) $\mu = 5$; and (b) $\mu = 10$. Note: 1 in = 25.4 mm.

Local and Global Ductility

Although the global ductility of the BRB has been considered to generate the design procedure, it is recognized that the governing design parameter in BRBs is the local ductility demand or strain in the yielding core. For long BRBs the ratio between the yield deformation of the brace to the yielding deformation of the yielding core, η, is close to one; however, for short BRBs, such as those required for this application, due to the specific internal design that these BRB may require, that ratio can increase to 1.70. In that case, targeting a ductility of 10 would translate into core ductility demands close to 17. Note that this may not always be the case, and this would have to be determined in collaboration with the BRB manufacturer. However, when that is an issue, to overcome this problem, the target ductility for BRBs in bridges could be calculated as function of the ductility in the core, μ_L. The global ductility in the braces, μ_g, can be calculated with Eq. (22), and this expression can be approximated by Eq. (23) for ductility demands of more than 7

$$\mu_g = [\mu_L + (\eta - 1)\beta(\mu_L)\omega(\mu_L)]\frac{1}{\eta} \tag{22}$$

$$\mu_g = \frac{\mu_L}{\eta} + 1 \tag{23}$$

ELF Design Procedure

On the strength of the results presented previously, it is possible to formulate the following proposed ELF procedure to design BRBs in the longitudinal direction. The steps of that design procedure are as follows:

1. Define the BRB length and BRB yield deformation. As a rule of thumb, the BRB length should be larger than 6% the span length (Wei and Bruneau 2018).
2. Define the target ductility of the brace, μ_{tg}, and check that the corresponding local ductility of the core is less than 10. Eqs. (22) or (23) can be used for this purpose.
3. Calculate the BRB target deformation corresponding to the values in Step 2.
4. Calculate the seismic mass of the span and pier stiffness.
5. Analyze one span as a SDOF system and find the period to reach the BRB target deformation using the following steps.
   a. Calculate the inelastic spectral displacement as:

$$\begin{aligned} S_d(T) &= R_d(T) \cdot g \cdot Sa(T) \cdot \left(\frac{T}{2\pi}\right)^2 \\ &= \frac{\mu_{tg}}{R(T)} \cdot g \cdot Sa(T) \cdot \left(\frac{T}{2\pi}\right)^2 \end{aligned} \tag{24}$$

where R(T) is given by Eq. (18) and assuming $\gamma_\mu = 1$, and R_d is the displacement amplification factor for short period

J. Struct. Eng., 2024, 150(3): 04024003

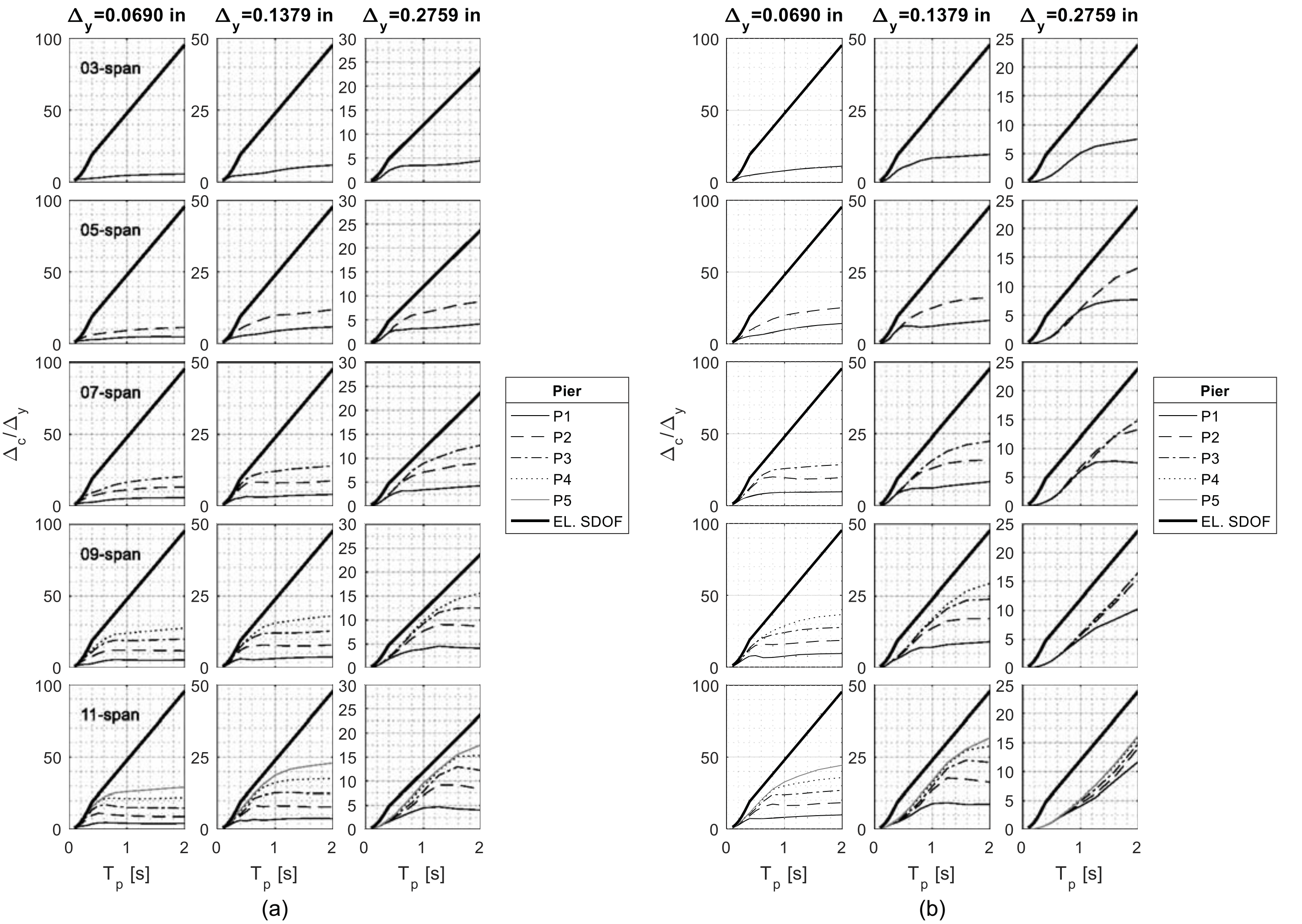

Fig. 14. Mean column displacement demand: (a) $\mu = 5$; and (b) $\mu = 10$. Note: 1 in = 25.4 mm.

system, $Sa(T)$ is the design spectrum, and g is the gravity acceleration.

b. Calculate the period of the SDOF, or also called the minimum period of the structure $T_{\min}$. The period of the SDOF is obtained by solving the following equation:

$$\Delta_y \cdot \mu_{tg} = S_d(T_{\min}) = \frac{\mu_{tg}}{R(T)} \cdot g \cdot Sa(T) \cdot \left(\frac{T}{2\pi}\right)^2 \quad (25)$$

$$\Delta_y = \frac{g \cdot Sa(T_{\min})}{R(T_{\min})} \cdot \left(\frac{T_{\min}}{2\pi}\right)^2 \quad (26)$$

The solution could be solved graphically by drawing the inelastic displacement spectrum and locating the period for which the BRB target deformation is obtained.

6. Calculate T_p, which is the period of one pier modeled as a SDOF with stiffness equal to the pier stiffness of the bridge and mass equal to the pier tributary mass in the bridge.

$$T_p = 2\pi\sqrt{\frac{M}{K_p}}$$

7. Calculate auxiliary parameters defined as:

$$\gamma = \frac{T_p}{T_{\min}} \quad (27a)$$

$$\lambda = 1 - \frac{8}{\gamma^2 + 8} \quad (27b)$$

$$\eta = \frac{T_1}{T_{\min}} = 1 + 0.4 \cdot \lambda \cdot N_{\text{span}} \quad (27c)$$

8. Calculate the period of the structure (T_1) in the longitudinal direction:

$$T_1 = \eta \cdot T_{\min} \quad (28)$$

9. Calculate the mode shape:

$$\phi(x, k_1, k_2) = 1 + y(x, k_1) - y(x, k_2)$$

$$x = 1 - 2\frac{i - 1}{N_{\text{span}} - 1}$$

$$y(x, k) = 1.0 - \left(0.60 + \frac{u_{tg}}{100}\right)\left[1 - \left(1 - \frac{|x|^{\frac{1}{k}}}{1.1}\right)^k\right]$$

$$k_1 = 4 \cdot \lambda \leq 0.15 \cdot (10 + \mu_{tg}) \cdot (1 - 0.7^{N_{\text{mas}} - 2}) \quad (29)$$

$$k_2 = 0.06(\gamma - 1) > 0 \quad (30)$$

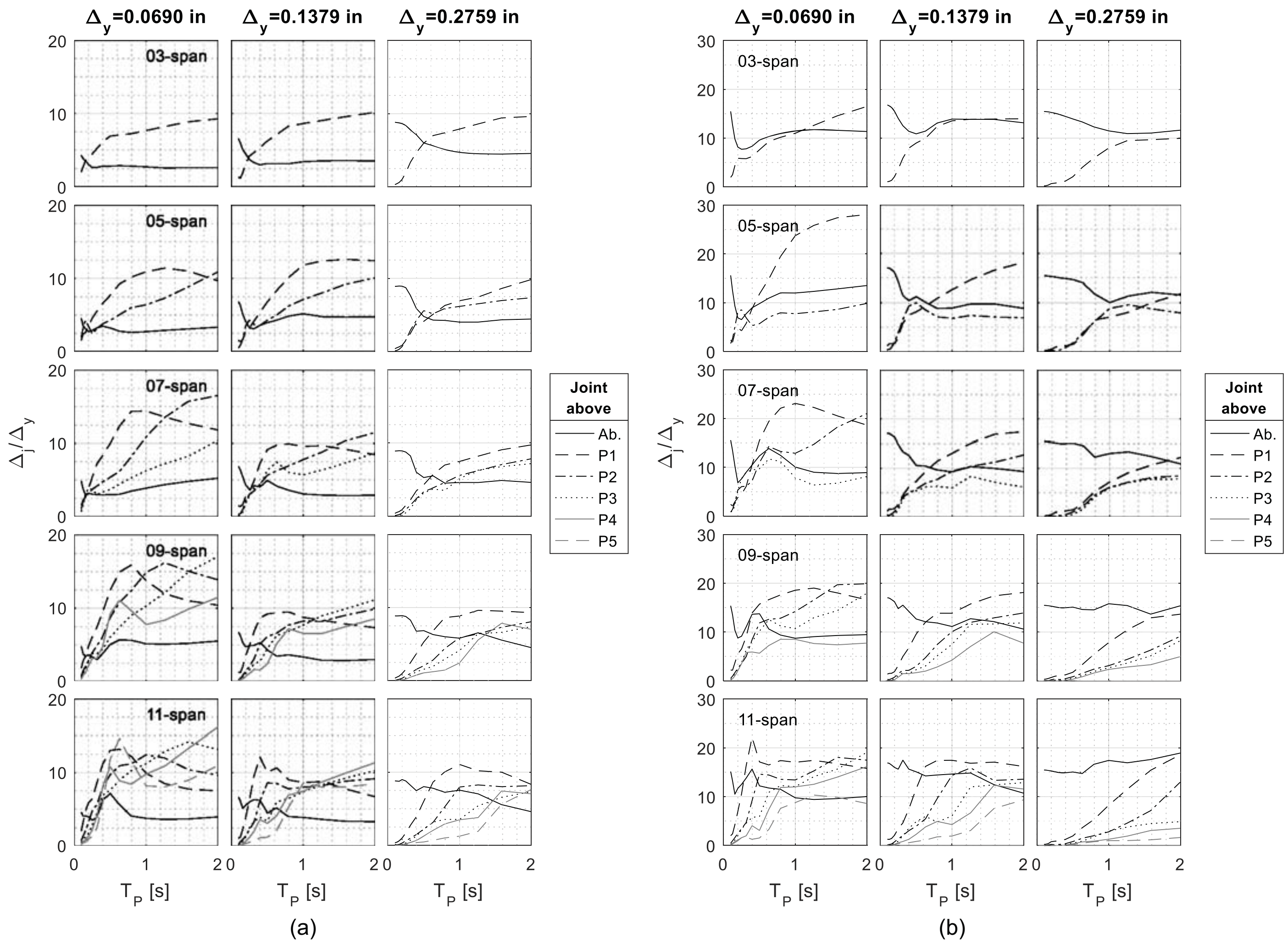

Fig. 15. 90th percentile expansion joint displacement demand: (a) $\mu = 5$; and (b) $\mu = 10$. Note: 1 in = 25.4 mm.

10. Calculate the reduction factor for the bridge:

$$1.0 \leq \alpha_\mu = 0.06\mu_{\text{SDOF}} + 0.7 \leq 1.3$$

$$\gamma_\mu = 2 \cdot \eta - 1 \leq 2 \tag{31}$$

$$R(T_1) = \begin{cases} \left(\dfrac{\mu_{\max}}{\alpha_\mu \gamma_\mu} - 1\right)\dfrac{T_1}{1.25T_s} + 1 & if\ T_1 < 1.25T_s \\ \dfrac{\mu_{\max}}{\alpha_\mu \gamma_\mu} & \text{otherwise} \end{cases}$$

11. Calculate the equivalent lateral force:

$$F_i = \frac{W\,Sa(T_1)}{R} \frac{m_i \phi(x_i)}{\sum_{j=1}^{n} m_j \phi(x_j)}$$

12. Calculate BRB cross-section areas.

An example of the application of this procedure is provided in the appendix.

Conclusions

A simplified design ELF procedure was proposed that can be used to obtain BRB ductility demands ranging from 5 to 10 (depending on the R-factor used). Using NL-RHA, the proposed ELF design procedure was found to provide acceptable results. The displacement demands in piers and expansion joints can be limited by an adequate selection of the BRB target ductility and BRB yield deformation. BRB demands obtained from the proposed ELF procedure were found to be acceptable, in spite of the method simplicity. Moreover, it was demonstrated by analyzing the fatigue damage in BRBs, that the possibility of BRB fracture due to a single earthquake is unlikely.

The proposed design procedure has the advantage of simplicity while being able to limit the ductility demand in BRBs along the bridge. Furthermore, it results in a design where the BRB ductility demand is relatively uniform along the length of the bridge.

Note that the work presented here has investigated the effectiveness of the procedure on regular multi-span bridges and future research will be needed to determine the range of applicability of this procedure to irregular bridges.

Appendix. Design Example for BRBs

To demonstrate the procedure described previously, a regular simply supported straight 5-span bridge is designed with BRBs in the longitudinal direction for a seismic region where the seismic design spectrum is the one shown in Fig. 16. Initially, the bridge was

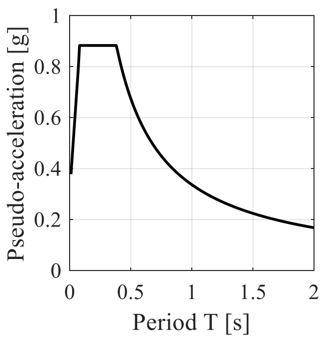

Fig. 16. Response spectrum.

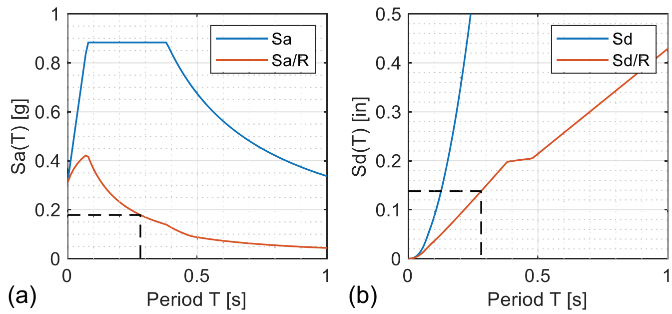

Fig. 17. Graphical solution: (a) spectral acceleration; and (b) spectral displacement. Note: 1 in = 25.4 mm.

analyzed as a multispan bridge without considering seismic forces. The weight of each floating span was calculated to be 386 kips (equal to a mass of 1 kip · s^2/in). The stiffness of piers was assumed to be 100 kip/in. In all piers, the base is fixed, and the top is simply connected to spans using slider bearings and BRBs. The lumped mass at the top of the pier is assumed equal to 38.6 kips (10% of the span mass). The calculated parameters in each iteration are provided in a table as follows. Design proceeds as follows:

1. The equivalent length of each BRB yielding core is selected to be 80 in, and their yield strength is 50 ksi.

$$\Delta_y = \frac{80 \text{ in}}{50 \text{ ksi}} = 0.138 \text{ in}$$

2. The target ductility demand in the BRB is selected to be 10.

$$\mu = 10$$

3. The BRB target deformation is:

$$\Delta_{\max} = \mu_{tg}\Delta_y = 1.38 \text{ in}$$

4. The span mass, M, is equal to 1 kip · s^2/in; and the pier stiffness, K_p, is equal to 100 kip/in.
5. Design of a SDOF system with mass equal to the span mass and a target displacement equal to $\Delta_{\max}$.

a. Calculation of the period of a SDOF system that reach the target deformation.

(1) Value of γ_μ with η equal to 1 (valid for a SDOF).

$$\gamma_\mu = 2\eta - 1 \leq 2.0$$

$$\gamma_\mu = 2 \cdot (1) - 1 = 1$$

$$\gamma_u = 1 \leq 2\, O.K.$$

(2) Value of α_μ

$$\alpha_u = 0.06\mu_{\text{SDOF}} + 0.7 \geq 1 \text{ if } \mu \leq 10$$

$$\alpha_u = 0.06 \cdot (10) + 0.7 = 1.3 \geq 1$$

$$\alpha_u = 1.3 \geq 1 O.K.$$

(3) Value of T_s

$$T_s = \frac{0.3371}{0.8833} = 0.3816s$$

(4) Definition of the values of the equation used to calculate R

$$R(T) = \begin{cases} \left(\dfrac{\mu_{tg}}{\alpha_u\gamma_\mu} - 1\right)\dfrac{T}{1.25T_s} + 1 & \text{if } T < 1.25T_s \\ \dfrac{\mu}{\alpha_u\gamma_\mu} & \text{otherwise} \end{cases}$$

$$R(T) = \begin{cases} \left(\dfrac{10}{1.3} - 1\right)\dfrac{T}{1.25 \cdot (0.3816)} + 1 & \text{if } T < 1.25T_s \\ \dfrac{10}{1.3} & \text{otherwise} \end{cases}$$

$$R(T) = \begin{cases} 14.03 \cdot T + 1 & \text{if } T < 0.477s \\ 7.69 & \text{otherwise} \end{cases}$$

(5) Calculation of the SDOF period by a graphical method. Fig. 17 shows the spectral acceleration for the design elastic spectrum and for the spectrum divided by R, and the corresponding displacement spectrum obtained from the acceleration spectrum. For a deformation equal to $\Delta_{\max}$ and to reach a target ductility equal to 10, the period of the SDOF system should be T_{SDOF} and is obtained from the figures using the reduced displacement spectrum (i.e., S_d/R). The period of the SDOF is then used to find the reduced spectral acceleration. These results are provided as follows:

$$T_{\min} = 0.281s$$

b. Define an initial BRB cross-section area. Any value can be used; however, the process followed here is a good first approximation. Thus, BRBs are designed for the span represented by the SDOF (one span with BRBs connected to rigid supports). Two BRBs are considered, one at each end. For a SDOF, the force in each BRB located at the end of the span is:

$$Sa_{\text{SDOF}}/R = 0.179g$$

$$F_{\text{BRB}_{\text{SDOF}}} = \frac{1}{2}\frac{Sa_{\text{SDOF}}}{R}W_{\text{span}} = \frac{1}{2} \cdot 0.179 \cdot 386 \text{ kips}$$
$$= 34.54 \text{ kips}$$

The cross-section area of each BRB is:

$$A_{\text{BRB}_{\text{SDOF}}} = \frac{F_{\text{BRB}_{\text{SDOF}}}}{F_y} = \frac{34.54 \text{ kips}}{50 \text{ ksi}} = 0.7 \text{ in}^2$$

J. Struct. Eng., 2024, 150(3): 04024003

Table 5. Calculation of equivalent lateral forces

Element	Mass (m) (kip · s^2/in)	x	$\phi(x)$	$m \cdot \phi(x)$	$\frac{m_i\phi(x_i)}{\Sigma m_j\phi(x_j)}$	$F_i = \frac{W\,Sa(T_1)}{R}\frac{m_i\phi(x_i)}{\Sigma m_j\phi(x_j)}$ (kip)
Span 1	1.0	−1.00	0.432	0.432	0.1421	52.13
Top pier 1	0.1	−0.75	0.382	0.038	0.0126	4.62
Span 2	1.0	−0.50	0.484	0.484	0.1595	58.51
Top pier 2	0.1	−0.25	0.644	0.064	0.0212	7.78
Span 3	1.0	0.00	1.000	1.000	0.3293	120.81
Top pier 3	0.1	0.25	0.644	0.064	0.0212	7.78
Span 4	1.0	0.50	0.484	0.484	0.1595	58.51
Top pier 4	0.1	0.75	0.382	0.038	0.0126	4.62
Span 5	1.0	1.00	0.432	0.432	0.1421	52.13
	5.4			3.037	1.0000	366.89

Note: 1 in = 25.4 mm, 1 kip = 4.448 kN, and 1 kip · s^2/in = 175.18 Mg.

6. Calculation of the parameter T_p

$$T_p = 2\pi\sqrt{\frac{M}{K_p}} = 2\pi\sqrt{\frac{1\text{ kip}\cdot\text{s}^2/\text{in}}{100\text{ kip/in}}} = 0.63s$$

7. Auxiliary parameters:

$$\gamma = \frac{T_p}{T_{\text{SDOF}}} = \frac{0.63s}{0.281s} = 2.242$$

$$\lambda = 1 - \frac{8}{\gamma^2+8} = 1 - \frac{8}{2.242^2+8} = 0.386$$

$$\eta = 1 + 0.4\cdot\lambda\cdot N_{\text{span}} = 1 + 0.4\cdot(0.386)\cdot(5) = 1.772$$

8. Approximation of the fundamental period of the bridge, T_1

$$T_1 = \eta\cdot T_{\text{SDOF}} = 1.772\cdot 0.281s = 0.498s$$

9. Definition of the equivalent mode shape
   a. Value of k_1

$$k_1 = 4\cdot\lambda = 4\cdot(0.386) = 1.544$$
$$\leq 0.15(10+\mu)(1-0.7^{N_{\text{span}}-2})$$

$$k_1 = 1.544 \leq 0.15(10+\mu)(1-0.7^{N_{\text{span}}-2})$$

$$k_1 = 1.544 \leq 0.15\cdot(10+10)\cdot(1-0.7^{5-2}) = 1.971$$

$$k_1 = 1.544 \leq 1.971$$

$$k_1 = 1.544$$

   b. Value of k_2

$$k_2 = 0.06\cdot(\gamma-1) > 0 = \max[0.06\cdot(\gamma-1), 0]$$

$$k_2 = \max[0.06\cdot(2.242-1), 0] = \max[0.0745, 0]$$

$$k_2 = 0.0745$$

   c. Definition of the equation of the mode shape

$$y(x,k) = 1 - \left(0.6 + \frac{\mu_{tg}}{100}\right)\left[1 - \left(1 - \frac{|x|^{\frac{1}{k}}}{1.1}\right)^k\right]$$
$$= 1 - \left(0.6 + \frac{10}{100}\right)\left[1 - \left(1 - \frac{|x|^{\frac{1}{k}}}{1.1}\right)^k\right]$$

$$y(x,k) = 1 - 0.7\left[1 - \left(1 - \frac{|x|^{\frac{1}{k}}}{1.1}\right)^k\right]$$
$$= 0.3 + 0.7(1 - 0.909\cdot|x|^{\frac{1}{k}})^k$$

$$\phi(x) = 1 + y(x,k_1) - y(x,k_2)$$

$$\phi(x) = 1 + 0.7(1 - 0.909\cdot|x|^{\frac{1}{k_1}})^{k_1}$$
$$- 0.7(1 - 0.909\cdot|x|^{\frac{1}{k_2}})^{k_2}$$

10. Calculation of the reduction factor for the multispan bridge.
   a. Value of γ_μ.

$$\gamma_\mu = 2\eta - 1 \leq 2.0$$

$$\gamma_\mu = \min[2\cdot(1.772)-1, 2] = \min[2.54, 2] = 2$$

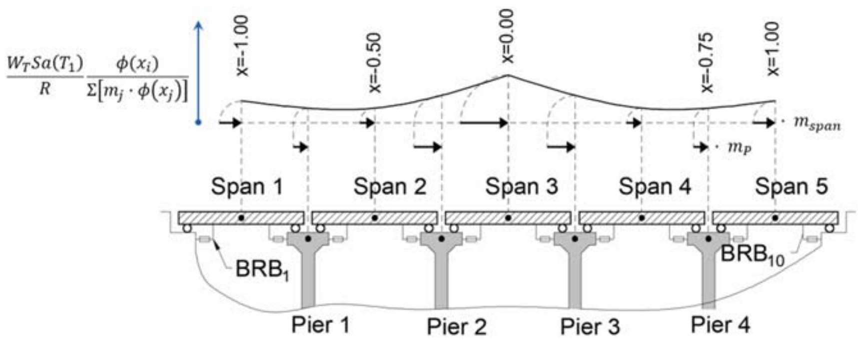

Fig. 18. Graphical representation of the equivalent mode shape and equivalent forces.

Table 6. BRB cross-section areas (in^2)

BRBs connected to	Iterations 0	1	2	3	Final design
Abutments	0.7	1.552	2.064	2.246	2.317
Pier 1	0.7	1.225	1.522	1.625	1.666
Pier 2	0.7	1.211	1.211	1.211	1.211

Note: 1 in = 25.4 mm.

b. Reduction factor. Since $T_1 \geq 1.25T_s$ then

$$R = \frac{\mu}{\alpha_u \cdot \gamma_\mu} = \frac{10}{(1.3)\cdot(2)} = 3.85$$

11. Calculation of the equivalent lateral forces. The equivalent forces are presented in Table 5. Fig. 18 is a sketch that shows graphically the shape of the mode shape and the distribution of forces.
  a. Calculation of the reduced spectral acceleration

$$\frac{Sa(T_1)}{R} = \frac{0.678}{3.85} = 0.176g$$

12. With the forces calculated in the previous step, the BRB cross-section areas are obtained by an iterative procedure. Any structural software could be used to calculate the forces in BRBs. For the first iteration (labeled iteration 0), $A_{\mathrm{BRB_{SDOF}}}$ is used as the cross-section area for all BRBs, but any cross-section area could be used in iteration 0. Forces in BRBs are calculated and the cross-section area is updated, then the model is updated with the new areas to recalculate forces in BRBs and redesign them, and the process is repeated until convergence is reached. For this example, four iterations were required to reach convergence. Cross-section areas for each iteration are shown in Table 6. If the mass of the pier cap is included in the step 3, the resulting cross-section areas would be between 1% and 5% smaller than those obtained in Table 6.

Data Availability Statement

Data generated during the study are available from the corresponding author by request.

Acknowledgments

This study was sponsored by the Transportation Research Board of the National Academies under the TRB-IDEA Program (NCHRP-215). The Fulbright program, SENESCYT Ecuador, and the University of Buffalo, are acknowledged for their financial support through a scholarship to Dr. Homero Carrion-Cabrera. However, any opinions, findings, conclusions, and recommendations presented are those of the authors and do not necessarily reflect the views of the sponsors.

References

AASHTO. 2011. *AASHTO guide specifications for LRFD seismic bridge design*. 2nd ed. Washington, DC: AASHTO.

Aiken, I. D., S. A. Mahin, and P. Uriz. 2002. "Large-scale testing of buckling-restrained braced frames." In *Proc., Japan Passive Control Symp*. Yokohama, Japan: Tokyo Institute of Technology.

Alfawakhiri, F., and M. Bruneau. 2001. "Local versus global ductility demands in simple bridges." *J. Struct. Eng.* 127 (5): 554–560. https://doi.org/10.1061/(ASCE)0733-9445(2001)127:5(554).

ASCE. 2017. *Minimum design loads and associated criteria for buildings and other structures*. ASCE/SEI 7-16. Reston, VA: ASCE.

Bruneau, M., and H. Carrion-Cabrera. 2020. "Buckling-restrained braces in bi-directional ductile diaphragms of multi-span bridges." In *Proc., The 17th World Conf. on Earthquake Engineering*. Tokyo: International Association of Earthquake Engineering.

Bruneau, M., C.-M. Uang, and S. R. Sabelli. 2011. *Ductile design of steel structures*. New York: McGraw-Hill Education.

Carden, L. P., A. M. Itani, and I. G. Buckle. 2006. "Seismic performance of steel girder bridges with ductile cross frames using buckling-restrained braces." *J. Struct. Eng.* 132 (3): 338–345. https://doi.org/10.1061/(ASCE)0733-9445(2006)132:3(338).

Carrion-Cabrera, H., and M. Bruneau. 2022a. Longitudinal-direction design of buckling restrained braces implemented to achieve resilient multi-span bridges. In *Proc., Institution of Civil Engineers-Bridge Engineering*, 1–28. Leeds, UK: ICE Publishing.

Carrion-Cabrera, H., and M. Bruneau. 2022b. "Seismic response of regular multi-span bridges having buckling-restrained braces in their longitudinal direction." *Eng. Struct.* 259 (Mar): 114127. https://doi.org/10.1016/j.engstruct.2022.114127.

Celik, O. C., and M. Bruneau. 2009. "Seismic behavior of bidirectional-resistant ductile end diaphragms with buckling restrained braces in straight steel bridges." *Eng. Struct.* 31 (2): 380–393. https://doi.org/10.1016/j.engstruct.2008.08.013.

Cui, J. 2020. *BRB performance issues*. Christchurch, New Zealand: Univ. of Canterbury.

Fahnestock, L. A., J. M. Ricles, and R. Sause. 2007. "Experimental evaluation of a large-scale buckling-restrained braced frame." *J. Struct. Eng.* 133 (9): 1205–1214. https://doi.org/10.1061/(ASCE)0733-9445(2007)133:9(1205).

Guerrero, H., T. Ji, A. Teran-Gilmore, and J. A. Escobar. 2016. "A method for preliminary seismic design and assessment of low-rise structures protected with Buckling-Restrained Braces." *Eng. Struct.* 123 (Mar): 141–154. https://doi.org/10.1016/j.engstruct.2016.05.015.

Hoveidae, N., and B. Rafezy. 2012. "Overall buckling behavior of all-steel buckling restrained braces." *J. Constr. Steel Res.* 79 (Dec): 151–158. https://doi.org/10.1016/j.jcsr.2012.07.022.

Kanaji, H., N. Hamada, T. Ishibashi, M. Amako, and T. Oryu. 2005. "Design and performance tests of buckling restrained braces for seismic retrofit of a long-span bridge." In *Proc., 21th US–Japan Bridge Engineering Workshop*. Tsukuba, Japan: Public Works Research Institute.

Kiggins, S., and C.-M. Uang. 2006. "Reducing residual drift of buckling-restrained braced frames as a dual system." *Eng. Struct.* 28 (11): 1525–1532. https://doi.org/10.1016/j.engstruct.2005.10.023.

Lanning, J. 2014. *Using buckling-restrained braces on long-span bridges near seismic faults*. San Diego: Univ. of California.

Lanning, J., G. Benzoni, and C.-M. Uang. 2016a. "Using buckling-restrained braces on long-span bridges. I: Full-scale testing and design implications." *J. Bridge Eng.* 21 (5): 04016001. https://doi.org/10.1061/(ASCE)BE.1943-5592.0000781.

Lanning, J., G. Benzoni, and C.-M. Uang. 2016b. "Using buckling-restrained braces on long-span bridges. II: Feasibility and development of a near-fault loading protocol." *J. Bridge Eng.* 21 (5): 04016002. https://doi.org/10.1061/(ASCE)BE.1943-5592.0000804.

Lehman, D. E., and J. P. Moehle. 2000. "Performance-based seismic design of reinforced concrete bridge columns." In *Proc., 12th World Conf. on Earthquake Engineering*. Upper Hutt, New Zealand: New Zealand Society for Earthquake Engineering.

Li, C.-H., Z. Vidmar, B. Saxey, M. Reynolds, and C.-M. Uang. 2022. "A procedure for assessing low-cycle fatigue life of buckling-restrained braces." *J. Struct. Eng.* 148 (2): 04021259. https://doi.org/10.1061/(ASCE)ST.1943-541X.0003237.

López, W. A., and R. Sabelli. 2004. "Seismic design of buckling-restrained braced frames." In *Steel tips*. Pleasant Hill, CA: Structural Steel Educational Council.

MacRae, G., C.-L. Lee, S. Vazquez-Coluga, J. Cui, S. Alizadeh, and L.-J. Jia. 2021. "BRB system stability considering frame out-of-plane

loading and deformation zone." *Bull. N.Z. Soc. Earthquake Eng.* 54 (1): 31–39. https://doi.org/10.5459/bnzsee.54.1.31-39.
Pantelides, C. P., L. Ibarra, Y. Wang, and A. Upadhyay. 2016. "Seismic rehabilitation of skewed and curved bridges using a new generation of buckling restrained braces." M. P. Consortium. Accessed November 10, 2020. https://rosap.ntl.bts.gov/view/dot/31880.
Reno, M. L., and M. N. Pohll. 2010. "Incorporating buckling restrained braces (BRB) as part of the Arburn-Foresthill bridge seismic retrofit." Accessed February 18, 2022. https://www.pwri.go.jp/eng/ujnr/tc/g/pdf/29/29-4-3_Reno.pdf.
Roussis, P. C., M. C. Constantinou, M. Erdik, E. Durukal, and M. Dicleli. 2003. "Assessment of performance of seismic isolation system of Bolu Viaduct." *J. Bridge Eng.* 8 (4): 182–190. https://doi.org/10.1061/(ASCE)1084-0702(2003)8:4(182).
Sabelli, R., S. Mahin, and C. Chang. 2003. "Seismic demands on steel braced frame buildings with buckling-restrained braces." *Eng. Struct.* 25 (5): 655–666. https://doi.org/10.1016/S0141-0296(02)00175-X.
Saxey, B. 2015. "A comparison of symmetric and non-symmetric loading on performance of buckling restrained braces." In *Proc., Steel Innovation Conf.* Auckland, New Zealand: Steel Construction.
Tremblay, R., P. Bolduc, R. Neville, and R. DeVall. 2006. "Seismic testing and performance of buckling-restrained bracing systems." *Can. J. Civ. Eng.* 33 (2): 183–198. https://doi.org/10.1139/l05-103.
Tsai, K. C., and P. C. Hsiao. 2008. "Pseudo-dynamic test of a full-scale CFT/BRB frame–Part II: Seismic performance of buckling-restrained braces and connections." *Earthquake Eng. Struct. Dyn.* 37 (7): 1099–1115. https://doi.org/10.1002/eqe.803.
Tsai, K. C., P. C. Hsiao, K. J. Wang, Y. T. Weng, M. L. Lin, K. C. Lin, C. H. Chen, J. W. Lai, and S. L. Lin. 2008. "Pseudo-dynamic tests of a full-scale CFT/BRB frame—Part I: Specimen design, experiment and analysis." *Earthquake Eng. Struct. Dyn.* 37 (7): 1081–1098. https://doi.org/10.1002/eqe.804.
Uang, C.-M., M. Nakashima, and K.-C. Tsai. 2004. "Research and application of buckling-restrained braced frames." *Int. J. Steel Struct.* 4 (4): 301–313.
Wang, Y., L. Ibarra, and C. Pantelides. 2016. "Seismic retrofit of a three-span RC bridge with buckling-restrained braces." *J. Bridge Eng.* 21 (11): 04016073. https://doi.org/10.1061/(ASCE)BE.1943-5592.0000937.
Watanabe, A., Y. Hitomi, E. Saeki, A. Wada, and M. Fujimoto. 1988. "Properties of brace encased in buckling-restraining concrete and steel tube." In *Proc., 9th World Conf. on Earthquake Engineering*, 719–724. Tokyo: International Association of Earthquake Engineering.
Wei, X., and M. Bruneau. 2016. *Buckling restrained braces applications for superstructure and substructure protection in bridges*. Amherst, NY: State Univ. of New York at Buffalo.
Wei, X., and M. Bruneau. 2018. "Experimental investigation of buckling restrained braces for bridge bidirectional ductile end diaphragms." *J. Struct. Eng.* 144 (6): 04018048. https://doi.org/10.1061/(ASCE)ST.1943-541X.0002042.
Zahrai, S. M., and M. Bruneau. 1999a. "Cyclic testing of ductile end diaphragms for slab-on-girder steel bridges." *J. Struct. Eng.* 125 (9): 987–996. https://doi.org/10.1061/(ASCE)0733-9445(1999)125:9(987).
Zahrai, S. M., and M. Bruneau. 1999b. "Ductile end-diaphragms for seismic retrofit of slab-on-girder steel bridges." *J. Struct. Eng.* 125 (1): 71–80. https://doi.org/10.1061/(ASCE)0733-9445(1999)125:1(71).

J. Struct. Eng., 2024, 150(3): 04024003